

Adaptive Beam Design for V2I Communications using Vehicle Tracking with Extended Kalman Filter

Seong-Hwan Hyun, *Student Member, IEEE*, Jiho Song, *Member, IEEE*, Keunwoo Kim, *Student Member, IEEE*, Jong-Ho Lee, *Member, IEEE*, and Seong-Cheol Kim, *Senior Member, IEEE*

Abstract—A vehicle-to-everything communication system is a strong candidate for improving the driving experience and automotive safety by linking vehicles to wireless networks. To guarantee the full benefits of vehicle connectivity, it is essential to ensure a stable network connection between the roadside unit (RSU) and fast-moving vehicles. Based on an extended Kalman filter (EKF), we develop a beam-tracking algorithm to enable reliable radio connections. For the vehicle tracking algorithm, we focus on estimating the rapid changes in the beam direction of a high-mobility vehicle while reducing the feedback overhead. Furthermore, we design a beamforming codebook that considers the road layout and RSU. By leveraging the proposed beamforming codebook, vehicles on the road can expect a service quality similar to that of conventional cellular services. Finally, a beamformer selection algorithm is developed to secure sufficient gain for a link budget. Numerical results verify that the EKF-based vehicle tracking algorithm and the proposed beamforming structure are more suitable for vehicle-to-infrastructure networks compared to existing schemes.

Index Terms—Vehicle tracking, vehicular mobility, extended Kalman filter, millimeter wave V2I communications

I. INTRODUCTION

Intelligent transportation system (ITS) has been considered an emerging technology that can improve the driving experience [1]–[3]. The objective of ITS is to enhance traffic efficiency and road safety by collecting sensor data associated with traffic conditions [4]. Although the sensor data allow each vehicle to increase situational awareness, the collected data should be shared between neighboring vehicles and/or the roadside unit (RSU) to facilitate fully automated driving. It is also necessary to obtain traffic information beyond the sensor range to build networks for connected vehicles. For these reasons, vehicle-to-everything (V2X) communication is a key technology for supporting ITS, because it enables vehicles to be aware of their surroundings via wireless links [5]–[8].

To ensure robust communications in V2X systems, it is essential to reevaluate wireless networks [9]. For road safety, low-latency and high-reliability are required to rapidly and accurately transmit warning messages about hazardous situations such as collisions. The challenge in V2X communication

S.-H. Hyun, K. Kim, and S.-C. Kim are with the School of Electrical Engineering, Seoul National University, Seoul 08826, South Korea (e-mail: {shhyun, kimkeunwoo15, sckim}@maxwell.snu.ac.kr).

J. Song (*corresponding author*) is with the School of Electrical Engineering, University of Ulsan, Ulsan 44610, South Korea (e-mail: jihosong@ulsan.ac.kr).

J.-H. Lee is with the School of Electronic Engineering, Soongsil University, Seoul 06978, South Korea (e-mail: jongho.lee@ssu.ac.kr).

This work has been submitted to the IEEE for possible publication. Copyright may be transferred without notice, after which this version may no longer be accessible.

systems is to meet these conflicting service requirements [10]. For example, obtaining high-resolution channel state information would help maintain a reliable network connection, but it also increases latency, which restricts the use of wireless resources, and vice versa.

Extensive data should be exchanged between RSU and vehicles to provide self-driving and platoon-based driving services [5], [11]. Using millimeter-wave (mmWave) systems with wide bandwidths is a lucrative solution for offering higher-than-expected data-rates in V2X communications. However, there are some obstacles to be addressed before providing vehicular communication services at mmWave frequencies [12]. Compared to conventional wireless networks operated in the ultra-high frequency (UHF) band, the mmWave band is more vulnerable to propagation conditions such as foliage, rainfall, and moisture in the air [13], [14]. Due to the short wavelength, the antenna cross-section becomes smaller, resulting in a larger path loss than with UHF signals. To compensate for the excessive propagation loss, it is necessary to consider a multi-antenna system for directive gain [15].

A highly narrow beamwidth for directional transmission enhances the beamforming gain, which may lead to intermittent radio link disconnections [16]. The high-mobility in V2X communications necessitates more beam training samples to reliably track vehicle movement. However, this beam alignment may significantly increase the beam training overhead. In order to resolve this trade-off problem, a vehicle tracking algorithm with a low overhead should be designed to make V2X communication systems robust to fast-moving vehicle environments [17], [18].

Vehicle tracking algorithms for mmWave broadband systems have been developed based on the extended Kalman filter (EKF) [18]–[20]. Although previous works in [18], [19] are eligible for estimating beam directions with moderate computational complexity, the vehicle tracking frameworks seem inappropriate because the dynamic state evolution model is designed as a linear function of beam directions [20]. The vehicle tracking algorithm in [20] is developed based on a realistic state evolution model, which describes the vehicle motion states, including position and velocity. However, the vehicle tracking algorithm can only estimate the beam direction in the vertical domain because the system model is developed based on a simplified (one-dimensional) geographic channel model. In practical vehicle-to-infrastructure (V2I) communication scenarios, it is even more important to estimate the beam direction in the horizontal domain because the transmit RSUs are deployed along the travel direction of vehicles. In this paper,

we model realistic road geometry for V2I communications to study a practical vehicle tracking framework. Based on the road geometry, we propose a vehicle tracking algorithm that can facilitate directional transmission by considering the beam directions in the vertical and horizontal domains.

EKF-based vehicle tracking algorithms are developed based on the linear approximation of the estimated channel vector [18]–[20]. Therefore, the vehicle tracking performance is highly dependent on the current beam estimate [21], [22]. Considering the sparse characteristics of mmWave channels, the channel training beamformer for the state update process should be carefully designed to maintain reliable vehicle tracking performance [23], [24]. The channel training beamformer in [20] is chosen from an array manifold set based on the current beam estimate. Since the beamformers are subject to the array manifold set, it is difficult to design the sounding signal according to the channel conditions. Specifically, in mmWave systems with multiple antennas, the beamwidth of the array response vector would be extremely narrow. However, in a low signal-to-noise ratio (SNR) regime, the array response vector with a narrow beamwidth intermittently disconnects a link for channel sounding because the spatial selectivity becomes more severe in mmWave systems. To improve the quality of sounding samples, we develop an adaptive channel sounding algorithm that can design the beam pattern of the beamformer according to the state prediction performance.

The conventional beamforming codebook is designed to achieve uniformly distributed beam directions considering the characteristics of the circular shape cellular service region [25]–[27]. However, in the V2I communication scenario, RSU is deployed near the road; therefore, the wireless service area is triangular. Due to the unusual shape of the service region, it is not reasonable to design a beamforming codebook based on the assumption that the beam directions are uniformly distributed. The beamforming codebook needs to be designed to reflect geographical features to offer a similar level of quality-of-service, regardless of the vehicle location on the road.

The objective of this work is to facilitate a large beamforming gain by designing beamforming codebooks that take into account geographical characteristics as well as selecting the most appropriate beamformer based on the vehicle position obtained through the EKF algorithm. The contributions of our paper are summarized as follows.

- *Vehicle tracking algorithm:* Since the relative velocity between a high-speed vehicle and RSU is significant, the beam direction towards the vehicle changes rapidly. RSU needs to know the vehicle motion state in real time to transmit a downlink signal in the right direction. The changes in the V2I channel direction can be updated based on a feedback-based vehicle tracking algorithm, although it would impose a burden on the feedback link. Under high-mobility scenarios, we develop a vehicle tracking algorithm that predicts a vehicle's motion state using uplink sounding signals with a small amount of vehicle motion feedback to RSU. In the proposed algorithm, an optimal combiner at RSU is computed to maximize the vehicle tracking performance through the uplink channel sounding process. Moreover, the acceleration parameter

estimation can further reduce the estimation uncertainty of the position and velocity information.

- *Beamformer design algorithm:* The wireless coverage in the V2I network is significantly different from those in conventional cellular networks. Since the majority of beamforming codebooks are designed based on conventional cellular network coverage, the beam pattern mapped to the geographical domain is severely distorted depending on the vehicle position. To resolve this problem, we develop a codebook design algorithm tailored for V2I communications, with road layout information that is not considered in the conventional beamforming codebook.
- *Beamformer selection algorithm:* Frequent beam switching can impose a burden on wireless communication systems with vehicular channels that vary rapidly with vehicle movement. It is not feasible to frequently recalculate the transmit beamformer. Considering that the beam switching speed at RSU is slower than that of a fast-moving vehicle, we develop a method to select the best transmit beamformer by predicting the future state vector of the vehicle based on the EKF algorithm.

The paper is organized as follows. In Section II, we present our system model. Based on an EKF algorithm, Section III proposes a vehicle tracking algorithm for V2I communication systems. In Section IV, we propose a transmit beamformer design algorithm to maximize the beam alignment and data-rate performance. We evaluate the proposed V2I communication system in Section V. Finally, Section VI details our conclusions.

Notation: \mathbb{C} is the field of complex numbers, \mathbb{R} the field of real numbers, $\mathcal{N}(m, \sigma^2)$ the normal distribution with mean m and variance σ^2 , $U(a, b)$ the uniform distribution in the range $[a, b]$, $E[\cdot]$ the expectation operator, $[a, b)$ the left-closed, right-open interval between a and b , $u(\cdot)$ the unit-step function, $|\cdot|$ the length of a range, $v(\cdot)$ the principal eigenvector of the matrix, $\text{Tr}\{\cdot\}$ the trace of the matrix, $\mathbf{1}_a$ the $a \times 1$ all ones column vector, $\mathbf{0}_a$ the $a \times 1$ all zeros column vector, $\mathbf{0}_{a \times b}$ the $a \times b$ all zeros matrix, \mathbf{I}_M the $M \times M$ identity matrix, and $\|\cdot\|_p$ the p -norm, respectively. Also, \mathbf{A}^{-1} , \mathbf{A}^H , \mathbf{A}^T , and $\mathbf{A}_{a,b}$ denote inverse, conjugate transpose, transpose, and (a, b) -th entry of the matrix \mathbf{A} , respectively.

II. SYSTEM MODEL

We consider a V2I wireless network in which RSU has M antennas, and a single antenna is mounted on the roof of each vehicle. The input-output expression for data transmission is defined by

$$r_\ell^{\text{down}} = \sqrt{\rho_\ell} \mathbf{h}_\ell^H \mathbf{c}_\ell s + n_\ell^{\text{down}}, \quad (1)$$

where $r_\ell^{\text{down}} \in \mathbb{C}$ is the received signal, $\mathbf{h}_\ell \in \mathbb{C}^M$ is the downlink multiple-input single-output channel vector, $\mathbf{c}_\ell \in \mathbb{C}^M$ is the unit-norm beamforming vector, s is the data symbol that is constrained by $E[|s|^2] = 1$ and $n_\ell^{\text{down}} \sim \mathcal{CN}(0, 1)$ is the additive white Gaussian noise. By assuming unit antenna gain at both the transmitter and the receiver, the average SNR can be defined by $\rho_\ell \doteq \frac{\varrho}{\sigma_n^2} \left(\frac{\lambda}{4\pi d_\ell} \right)^n$, where ϱ , σ_n^2 , λ , d_ℓ and n denote the transmit power, noise power, wavelength of the radio signals, distance between the vehicle, and RSU and the path-loss exponent, respectively.

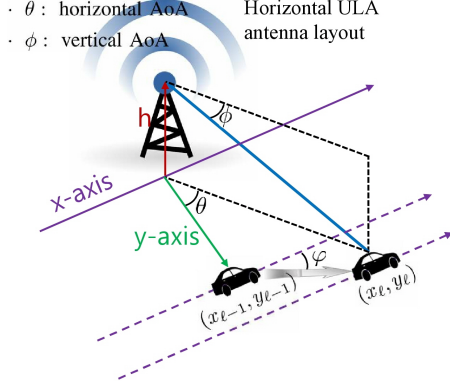


Fig. 1. V2I communication system overview.

We consider a hybrid beamforming system in which N radio frequency chains are connected to a baseband beamforming unit [28], [29]. The RF chain generates a unit-norm analog beamsteering vector, $\mathbf{f}_n \in \mathbb{C}^M$, consisting of M equal gain complex numbers. The beamforming vector is constructed by combining N analog beamsteering vectors with a unit-norm digital weight vector, $\mathbf{v} \in \mathbb{C}^N$, such that $\mathbf{c}_\ell = [\mathbf{f}_1, \dots, \mathbf{f}_N] \mathbf{v}$.

With a single-beam channel model at mmWave bands, the channel vector can be represented as a function of the beam direction of the dominant radio path ψ_ℓ , such that $\mathbf{h}_\ell = \mathbf{h}(\psi_\ell)$. At discrete time ℓ , the input-output expression for downlink transmissions is then rewritten as

$$r_\ell^{\text{down}} = \sqrt{\rho_\ell} (\beta_\ell \mathbf{d}_M(\psi_\ell))^H \mathbf{c}_\ell s + n_\ell^{\text{down}},$$

where $\beta_\ell \sim \mathcal{CN}(0, 1)$ denotes the small-scale channel fading parameter. If we consider a uniform linear array (ULA) layout, then the array response vector can be modeled as $\mathbf{d}_M(\psi_\ell) = [1, e^{j\psi_\ell}, \dots, e^{j(M-1)\psi_\ell}]^T \in \mathbb{C}^M$.

The transmitter mounted on RSU sends the data symbol to a vehicle in the traffic lane. As depicted in Fig. 1, the height of RSU is given by h , distance from RSU to a vehicle (on the y -axis) is defined by y_ℓ , and position of the vehicle at discrete time ℓ in the moving direction (x -axis), is denoted as x_ℓ . Based on the road layout, the horizontal angle of departure (AoD) is defined as $\sin \theta = x(x^2 + y^2)^{-\frac{1}{2}}$, and the vertical AoD is defined as $\cos \phi = (x^2 + y^2)^{\frac{1}{2}}(x^2 + y^2 + h^2)^{-\frac{1}{2}}$. For the ULA scenario, the spatial frequency in the angular domain is then written as

$$\psi = \pi \sin \theta \cos \phi = \pi x(x^2 + y^2 + h^2)^{-\frac{1}{2}} \doteq T(x, y). \quad (2)$$

In this paper, we make the following assumptions:

- The initial position and velocity information of the vehicle (x_0, y_0, v_0) is reported to RSU via a feedback link.
- Large-scale and small-scale channel fading parameters (ρ_ℓ, β_ℓ) are known at RSU.

III. VEHICLE TRACKING ALGORITHM

The direction of the dominant radio path from RSU to the vehicles changes significantly due to their high-mobility. Thus, it is necessary to quickly find the proper beamformer to support high-mobility scenarios in vehicular communication networks. The channel direction to the vehicle can be obtained by

providing RSU with immediate feedback on the vehicle motion states, including position and velocity. However, the feedback-assisted state tracking approach may lead to a significant increase in the control signaling overhead in wireless networks. Considering a high-mobility scenario, it is not practical to frequently communicate vehicle motion states via feedback links. We develop a vehicle tracking algorithm using uplink channel sounding to estimate vehicle motion states without relying on a direct feedback process.

1) *Linear state prediction*: The state vector of a moving vehicle is defined by, $\mathbf{t}_\ell = [x_\ell, y_\ell, v_\ell]^T \in \mathbb{R}^3$, where x_ℓ , y_ℓ , and v_ℓ , denote the positions on the x -axis, y -axis, and velocity of the vehicle at time ℓ , respectively. The linear state prediction model at discrete time ℓ with step T_s is modeled by

$$\mathbf{t}_\ell = \mathbf{A} \mathbf{t}_{\ell-1} + \mathbf{b} \alpha + \mathbf{c}_{\ell-1}, \quad (3)$$

where $\mathbf{A} = \begin{bmatrix} 1 & 0 & T_s \cos \varphi \\ 0 & 1 & T_s \sin \varphi \\ 0 & 0 & 1 \end{bmatrix} \in \mathbb{R}^{3 \times 3}$ is the state transition matrix, $\mathbf{b} = \left[\frac{T_s^2}{2} \cos \varphi, \frac{T_s^2}{2} \sin \varphi, T_s \right]^T \in \mathbb{R}^3$ is the acceleration transition vector with the covariance matrix $\mathbf{Q}_\alpha = \mathbf{b} \mathbf{b}^T \sigma_\alpha^2$, as in [30]. Similar to [20], [24], the error transition vector is modeled using $\mathbf{c}_{\ell-1} \sim \mathcal{N}(\mathbf{0}_3, \mathbf{Q}_\omega)$ with the covariance matrix $\mathbf{Q}_\omega = \text{diag}[T_s^2 \sigma_\omega^2 \cos^2 \varphi, T_s^2 \sigma_\omega^2 \sin^2 \varphi, \sigma_\omega^2]$, where σ_ω^2 is the variance of the error parameter. Note that $\varphi \in [-\pi/2, \pi/2]$ denotes the vehicle steering angle and $\alpha \sim \mathcal{N}(0, \sigma_\alpha^2)$ denotes the acceleration parameter that follows Gaussian random process. In each coherence period, the acceleration parameter is assumed to be stationary, whereas the error parameter is dynamic. Furthermore, we assume that the acceleration parameter is independent of the error parameter.

2) *State tracking based on uplink sounding*: RSU only knows the state transition matrix and the initial state vector¹, so the uncertainty of the predicted state vector will gradually increase, without correcting the error transition vectors in (3). It is necessary to predict the acceleration parameter and the error parameter in order to update the state vector precisely. We focus on estimating two random parameters that affect the motion state vector using uplink channel sounding signals.

Assuming a time division duplexing architecture, the uplink channel sounding process for discrete time ℓ is

$$r_\ell = \mathbf{z}_\ell \mathbf{h}(\psi_\ell) + n_\ell, \quad (4)$$

where $\mathbf{z}_\ell \in \mathbb{C}^{1 \times M}$ is the unit-norm combiner at RSU, $r_\ell \in \mathbb{C}$ is the combined baseband signal, $\mathbf{h}(\psi_\ell) = \beta_\ell \mathbf{d}_M(\psi_\ell) \in \mathbb{C}^M$ is the uplink channel vector, and $n_\ell = \mathbf{z}_\ell \mathbf{n}_\ell \sim \mathcal{CN}(0, \rho_\ell^{-1})$ is the combined noise signal that hinders correct channel sounding. The variables in (4) can be reformulated using real and imaginary parts, such that $r_\ell = r_\ell^{\text{re}} + i r_\ell^{\text{im}}$, $\mathbf{z}_\ell = \mathbf{z}_\ell^{\text{re}} + i \mathbf{z}_\ell^{\text{im}}$, $\beta_\ell = \beta_\ell^{\text{re}} + i \beta_\ell^{\text{im}}$, and $n_\ell = n_\ell^{\text{re}} + i n_\ell^{\text{im}}$. Furthermore, the array response vector is rewritten as $\mathbf{d}_M(\psi_\ell) = \mathbf{d}_M^{\text{re}}(\psi_\ell) + i \mathbf{d}_M^{\text{im}}(\psi_\ell)$, where the real and imaginary parts of the array vector are

$$\mathbf{d}_M^{\text{re}}(\psi_\ell) = [\cos(0), \cos(\psi_\ell), \dots, \cos((M-1)\psi_\ell)]^T, \quad (5)$$

$$\mathbf{d}_M^{\text{im}}(\psi_\ell) = [\sin(0), \sin(\psi_\ell), \dots, \sin((M-1)\psi_\ell)]^T. \quad (6)$$

¹An initial state vector, $\mathbf{t}_0 = [x_0, y_0, v_0]^T$, is fed back to RSU at the beginning of a vehicle tracking process. An initial feedback error is modelled by $\mathbf{e}_\epsilon = \epsilon \mathbf{t}_0$, where $\epsilon \sim \mathcal{N}(0, \sigma_\epsilon^2)$ denotes the feedback error parameter.

A Kalman filter estimates the state vector by iteratively applying two steps: a dynamic update based on the state prediction model in (3); and a measurement update using the uplink sounding sample in (4). The state prediction process updating the position and velocity information is defined in the real domain, whereas the uplink sounding process in (4) is defined in the complex domain. During the measurement update process, an innovation term that contains new information about the state vector is added to the previous state vector. However, since measurement noise hinders an accurate estimation, the complex noise, which makes the state vector complex, would remain in the innovation term.

To conduct the state prediction and update processes in the same domain, the uplink channel sounding process in (4) is rewritten in the real domain, such that

$$\tilde{\mathbf{r}}_\ell = \tilde{\mathbf{Z}}_\ell \tilde{\mathbf{h}}(\psi_\ell) + \tilde{\mathbf{n}}_\ell, \quad (7)$$

where all variables in the real domain are reformulated as follows: $\tilde{\mathbf{r}}_\ell = [r_\ell^{\text{re}}, r_\ell^{\text{im}}]^T \in \mathbb{R}^2$, $\tilde{\mathbf{Z}}_\ell = \begin{bmatrix} \mathbf{z}_\ell^{\text{re}} & -\mathbf{z}_\ell^{\text{im}} \\ \mathbf{z}_\ell^{\text{im}} & \mathbf{z}_\ell^{\text{re}} \end{bmatrix} \in \mathbb{R}^{2 \times 2M}$, and $\tilde{\mathbf{n}}_\ell = [n_\ell^{\text{re}}, n_\ell^{\text{im}}]^T \in \mathbb{R}^2$. The channel vector is reformulated as

$$\tilde{\mathbf{h}}(\psi_\ell) = \begin{bmatrix} \mathbf{h}^{\text{re}}(\psi_\ell) \\ \mathbf{h}^{\text{im}}(\psi_\ell) \end{bmatrix} = \begin{bmatrix} \beta_\ell^{\text{re}} \mathbf{d}_M^{\text{re}}(\psi_\ell) - \beta_\ell^{\text{im}} \mathbf{d}_M^{\text{im}}(\psi_\ell) \\ \beta_\ell^{\text{im}} \mathbf{d}_M^{\text{re}}(\psi_\ell) + \beta_\ell^{\text{re}} \mathbf{d}_M^{\text{im}}(\psi_\ell) \end{bmatrix}.$$

The uplink channel sounding in (7) is represented by a simplified single-input multiple-output channel vector. The simplified channel vector is defined using the array response vectors in (5) and (6), which are the nonlinear functions of the beam direction (spatial frequency). Furthermore, the beam direction is defined based on equation (2), which is given as a nonlinear function of the position variables. Thus, the uplink channel sounding is given as a nonlinear function of the position variables.

The Kalman filter that is typically discussed directly applies only to linear systems. Nonlinearity exists between uplink sounding and vehicle position in our case. Therefore, the uplink channel sounding expression needs to be linearized. As depicted in Fig. 1, the beam direction (spatial frequency) at time ℓ is defined as a function of the position variable in the state vector, such that $\psi_\ell = \pi x_\ell (x_\ell^2 + y_\ell^2 + h^2)^{-\frac{1}{2}} \doteq g(\mathbf{t}_\ell)$, and the channel vector is then redefined as $\tilde{\mathbf{h}}(g(\mathbf{t}_\ell))$. At time ℓ , the first-order Taylor series approximation of the channel vector for the predicted state vector $\hat{\mathbf{t}}_{\ell|\ell-1}$ is given by

$$\tilde{\mathbf{h}}(g(\mathbf{t}_\ell)) \simeq \tilde{\mathbf{h}}(g(\hat{\mathbf{t}}_{\ell|\ell-1})) + \tilde{\mathbf{D}}_{\ell|\ell-1}(\mathbf{t}_\ell - \hat{\mathbf{t}}_{\ell|\ell-1}), \quad (8)$$

where the Jacobian matrix of the channel vector, $\tilde{\mathbf{D}}_{\ell|\ell-1} = \frac{\partial \tilde{\mathbf{h}}(g(\mathbf{t}))}{\partial \mathbf{t}} \Big|_{\mathbf{t}=\hat{\mathbf{t}}_{\ell|\ell-1}}$, is derived from Proposition 1.

Proposition 1: The Jacobian matrix of the channel vector is

$$\tilde{\mathbf{D}}_{\ell|\ell-1} = \begin{bmatrix} \dot{\mathbf{h}}^{\text{re}}(g(\hat{\mathbf{t}}_{\ell|\ell-1})) \\ \dot{\mathbf{h}}^{\text{im}}(g(\hat{\mathbf{t}}_{\ell|\ell-1})) \end{bmatrix} \dot{g}(\hat{\mathbf{t}}_{\ell|\ell-1})$$

where $\dot{g}(\hat{\mathbf{t}}_{\ell|\ell-1}) \doteq \frac{\pi[(\hat{y}_{\ell|\ell-1}^2 + h^2), -\hat{x}_{\ell|\ell-1} \hat{y}_{\ell|\ell-1}, \cos \varphi(\hat{y}_{\ell|\ell-1}^2 + h^2) T_s]}{(\hat{x}_{\ell|\ell-1}^2 + \hat{y}_{\ell|\ell-1}^2 + h^2)^{\frac{3}{2}}}$, $\dot{\mathbf{h}}^{\text{re}}(\psi_\ell) \doteq \frac{\partial \mathbf{h}^{\text{re}}(\psi)}{\partial \psi} \Big|_{\psi=\psi_\ell} = \beta_\ell^{\text{re}} \dot{\mathbf{d}}_M^{\text{re}}(\psi_\ell) - \beta_\ell^{\text{im}} \dot{\mathbf{d}}_M^{\text{im}}(\psi_\ell)$, and $\dot{\mathbf{h}}^{\text{im}}(\psi_\ell) \doteq \frac{\partial \mathbf{h}^{\text{im}}(\psi)}{\partial \psi} \Big|_{\psi=\psi_\ell} = \beta_\ell^{\text{im}} \dot{\mathbf{d}}_M^{\text{re}}(\psi_\ell) + \beta_\ell^{\text{re}} \dot{\mathbf{d}}_M^{\text{im}}(\psi_\ell)$.

Proof: The Jacobian matrix of the simplified channel vector is obtained by solving the equation $\tilde{\mathbf{D}}_{\ell|\ell-1} = \frac{\partial \tilde{\mathbf{h}}(g(\mathbf{t}))}{\partial \mathbf{t}} \Big|_{\mathbf{t}=\hat{\mathbf{t}}_{\ell|\ell-1}}$. Based on the chain rule, the partial derivative of the channel vector in the beam direction, $\hat{\mathbf{t}}_{\ell|\ell-1}$, is divided into two parts, such that $\tilde{\mathbf{D}}_{\ell|\ell-1} = \frac{\partial \tilde{\mathbf{h}}(\psi)}{\partial \psi} \Big|_{\psi=g(\hat{\mathbf{t}}_{\ell|\ell-1})} \frac{\partial g(\mathbf{t})}{\partial \mathbf{t}} \Big|_{\mathbf{t}=\hat{\mathbf{t}}_{\ell|\ell-1}}$. The first part is derived as

$$\frac{\partial \tilde{\mathbf{h}}(\psi)}{\partial \psi} \Big|_{\psi=\psi_\ell} = \begin{bmatrix} \beta_\ell^{\text{re}} \dot{\mathbf{d}}_M^{\text{re}}(\psi_\ell) - \beta_\ell^{\text{im}} \dot{\mathbf{d}}_M^{\text{im}}(\psi_\ell) \\ \beta_\ell^{\text{im}} \dot{\mathbf{d}}_M^{\text{re}}(\psi_\ell) + \beta_\ell^{\text{re}} \dot{\mathbf{d}}_M^{\text{im}}(\psi_\ell) \end{bmatrix},$$

where the partial derivatives of the real and imaginary parts of the array response vector are

$$\dot{\mathbf{d}}_M^{\text{re}}(\psi_\ell) = [0, -\sin(\psi_\ell), \dots, -(M-1) \sin((M-1)\psi_\ell)]^T, \\ \dot{\mathbf{d}}_M^{\text{im}}(\psi_\ell) = [0, \cos(\psi_\ell), \dots, (M-1) \cos((M-1)\psi_\ell)]^T.$$

Furthermore, the second part is derived as

$$\frac{\partial g(\mathbf{t})}{\partial \mathbf{t}} = \left[\frac{\partial g(\mathbf{t})}{\partial x}, \frac{\partial g(\mathbf{t})}{\partial y}, \frac{\partial g(\mathbf{t})}{\partial v} \right] \Big|_{\mathbf{t}=[x, y, v]^T} \\ \stackrel{(a)}{\simeq} \frac{\pi[(y^2 + h^2), -xy, (y^2 + h^2)T_s \cos \varphi]}{(x^2 + y^2 + h^2)^{\frac{3}{2}}},$$

where (a) is derived because $\frac{\partial x}{\partial v} \simeq T_s \cos \varphi$. \blacksquare

By substituting the approximated channel vector in (8) into (7), the input-output expression for uplink channel sounding can be approximated by

$$\tilde{\mathbf{r}}_\ell \simeq \tilde{\mathbf{Z}}_\ell \tilde{\mathbf{D}}_{\ell|\ell-1} \mathbf{t}_\ell + \tilde{\mathbf{Z}}_\ell \tilde{\mathbf{h}}(g(\hat{\mathbf{t}}_{\ell|\ell-1})) - \tilde{\mathbf{Z}}_\ell \tilde{\mathbf{D}}_{\ell|\ell-1} \hat{\mathbf{t}}_{\ell|\ell-1} + \tilde{\mathbf{n}}_\ell. \quad (9)$$

Similar to [20]–[22], we can develop EKF by putting the rewritten equation in (9) into the Kalman filter, instead of exploiting the nonlinear channel sounding equation in (7).

Based on the state transition model in (3), the state vector and covariance matrix can be updated as $\hat{\mathbf{t}}_{\ell|\ell-1} = \mathbf{A} \hat{\mathbf{t}}_{\ell-1} + \mathbf{Q}_{\ell|\ell-1} = \mathbf{A} \hat{\mathbf{t}}_{\ell-1} + \mathbf{Q}_\alpha + \mathbf{Q}_\omega$, respectively. Since the acceleration and error parameters cannot be corrected in the state prediction process, the uncertainty of the state vector gradually increases. To correct the prediction errors, the state vector and the covariance matrix should be updated based on the EKF algorithm. The updated state vector is given by

$$\hat{\mathbf{t}}_\ell = \hat{\mathbf{t}}_{\ell|\ell-1} + \tilde{\mathbf{K}}_\ell (\tilde{\mathbf{r}}_\ell - \tilde{\mathbf{Z}}_\ell \tilde{\mathbf{h}}(g(\hat{\mathbf{t}}_{\ell|\ell-1}))),$$

and the updated covariance matrix is given by

$$\mathbf{Q}_\ell = (\mathbf{I}_3 - \tilde{\mathbf{K}}_\ell \tilde{\mathbf{Z}}_\ell \tilde{\mathbf{D}}_{\ell|\ell-1}) \mathbf{Q}_{\ell|\ell-1},$$

in which the Kalman gain matrix is defined by

$$\tilde{\mathbf{K}}_\ell = \mathbf{Q}_{\ell|\ell-1} \tilde{\mathbf{D}}_{\ell|\ell-1}^T \tilde{\mathbf{Z}}_\ell^T \left(\tilde{\mathbf{Z}}_\ell \tilde{\mathbf{D}}_{\ell|\ell-1} \mathbf{Q}_{\ell|\ell-1} \tilde{\mathbf{D}}_{\ell|\ell-1}^T \tilde{\mathbf{Z}}_\ell^T + \frac{\mathbf{I}_2}{2\rho_\ell} \right)^{-1}. \quad (10)$$

The Kalman gain matrix is designed to optimize the state prediction and update process by considering both the state transition process and the approximated channel sounding expression together [21], [22].

3) Combining vector design for uplink channel sounding:

We develop a method for computing the optimal combiner for the uplink sounding process. The objective of the combining process is to design a combiner that maximizes the overall state estimation performance of the EKF algorithm. As studied in [23], [24], we aim to compute an optimal combiner at RSU that minimizes the trace of the covariance matrix. The combiner is constructed by computing the real and imaginary parts of the combined vector in the real domain, such that

$$\begin{aligned}
(\mathbf{z}_\ell^{\text{re}}, \mathbf{z}_\ell^{\text{im}}) &= \arg \min_{\bar{\mathbf{z}}_\ell^{\text{re}}, \bar{\mathbf{z}}_\ell^{\text{im}}} \text{Tr}\{\mathbf{Q}_\ell\} \\
&= \arg \max_{\bar{\mathbf{z}}_\ell^{\text{re}}, \bar{\mathbf{z}}_\ell^{\text{im}}} \text{Tr}\{\tilde{\mathbf{K}}_\ell \bar{\mathbf{Z}}_\ell \tilde{\mathbf{D}}_{\ell|\ell-1} \mathbf{Q}_{\ell|\ell-1}\} \\
&= \arg \max_{\bar{\mathbf{z}}_\ell^{\text{re}}, \bar{\mathbf{z}}_\ell^{\text{im}} \in \mathbb{R}^{1 \times M}} \text{Tr}\{\mathbf{Q}_{\ell|\ell-1} \tilde{\mathbf{D}}_{\ell|\ell-1}^T \bar{\mathbf{Z}}_\ell^T \Lambda_{\ell, \rho_\ell}^{-1} \bar{\mathbf{Z}}_\ell \tilde{\mathbf{D}}_{\ell|\ell-1} \mathbf{Q}_{\ell|\ell-1}\} \\
&\stackrel{(a)}{=} \arg \max_{\bar{\mathbf{z}}_\ell^{\text{re}}, \bar{\mathbf{z}}_\ell^{\text{im}} \in \mathbb{R}^{1 \times M}} \text{Tr}\{\Lambda_\ell^{-1} \bar{\mathbf{Z}}_\ell \tilde{\mathbf{D}}_{\ell|\ell-1} \mathbf{Q}_{\ell|\ell-1}^2 \tilde{\mathbf{D}}_{\ell|\ell-1}^T \bar{\mathbf{Z}}_\ell^T\}, \quad (11)
\end{aligned}$$

where $\Lambda_\ell \doteq (\bar{\mathbf{Z}}_\ell \tilde{\mathbf{D}}_{\ell|\ell-1} \mathbf{Q}_{\ell|\ell-1} \tilde{\mathbf{D}}_{\ell|\ell-1}^T \bar{\mathbf{Z}}_\ell^T + \mathbf{I}_2/(2\rho_\ell))$, the combining matrix in the real domain is defined by $\bar{\mathbf{Z}}_\ell = \begin{bmatrix} \bar{\mathbf{z}}_\ell^{\text{re}} & -\bar{\mathbf{z}}_\ell^{\text{im}} \\ \bar{\mathbf{z}}_\ell^{\text{im}} & \bar{\mathbf{z}}_\ell^{\text{re}} \end{bmatrix}$, and (a) is derived as $\text{Tr}\{\mathbf{AB}\} = \text{Tr}\{\mathbf{BA}\}$ [31].

However, in the real domain, it is not easy to jointly compute the real and imaginary parts of the combining vector. Therefore, we rewrite the problem in (11) as an optimization problem in the complex domain, such that

$$\begin{aligned}
\mathbf{z}_\ell &= \arg \max_{\bar{\mathbf{z}} \in \mathbb{C}^{1 \times M}} \frac{\bar{\mathbf{z}}(\mathbf{D}_{\ell|\ell-1} \mathbf{Q}_{\ell|\ell-1}^2 \mathbf{D}_{\ell|\ell-1}^H) \bar{\mathbf{z}}^H}{\bar{\mathbf{z}}(\mathbf{D}_{\ell|\ell-1} \mathbf{Q}_{\ell|\ell-1} \mathbf{D}_{\ell|\ell-1}^H + \mathbf{I}_M/\rho_\ell) \bar{\mathbf{z}}^H} \\
&\stackrel{(a)}{=} \mathbf{v}\left\{(\mathbf{D}_{\ell|\ell-1} \mathbf{Q}_{\ell|\ell-1} \mathbf{D}_{\ell|\ell-1}^H + \mathbf{I}_M/\rho_\ell)^{-1} (\mathbf{D}_{\ell|\ell-1} \mathbf{Q}_{\ell|\ell-1}^2 \mathbf{D}_{\ell|\ell-1}^H)\right\}, \quad (12)
\end{aligned}$$

where $\mathbf{D}_{\ell|\ell-1} = \left[\frac{\partial \mathbf{h}^{\text{re}}(\psi)}{\partial \psi} + i \frac{\partial \mathbf{h}^{\text{im}}(\psi)}{\partial \psi} \right] \Big|_{\psi=g(\hat{\mathbf{t}}_{\ell|\ell-1})} \dot{g}(\mathbf{t}) \Big|_{\mathbf{t}=\hat{\mathbf{t}}_{\ell|\ell-1}}$, $\bar{\mathbf{z}} = \bar{\mathbf{z}}_\ell^{\text{re}} + i \bar{\mathbf{z}}_\ell^{\text{im}}$ and (a) are derived based on the Rayleigh quotient algorithm [32]. The hybrid beamforming system at RSU might not be able to construct the optimal combiner in (12), due to an equal gain constraint on the analog beamforming hardware [28], [29]. A complex combiner should be reconstructed to satisfy the power constraint of the hybrid beamforming setup. To generate a complex combiner close to the optimal combiner, a set of analog beamsteering vectors and a digital weight vector are constructed based on the orthogonal matching pursuit algorithm. Please refer to [28], [29], [33], [34] for the hybrid combiner design problem. Finally, the complex combiner $\mathbf{z}_\ell = \mathbf{z}_\ell^{\text{re}} + i \mathbf{z}_\ell^{\text{im}}$ is then reformulated in the real domain as $\tilde{\mathbf{Z}}_\ell = \begin{bmatrix} \mathbf{z}_\ell^{\text{re}} & -\mathbf{z}_\ell^{\text{im}} \\ \mathbf{z}_\ell^{\text{im}} & \mathbf{z}_\ell^{\text{re}} \end{bmatrix}$, and the matrix is used to rewrite the uplink sounding signal, as in (7).

4) Acceleration parameter estimation: The proposed vehicle tracking algorithm aims to correct the errors between the actual state vector and predicted state vector caused by the acceleration and error variables. The vehicle tracking algorithm sequentially corrects the errors with the aid of the uplink channel sounding process. If we estimate the acceleration parameter successfully, then we can focus on correcting the errors via Kalman filtering, because the acceleration parameter is assumed to be stationary

in each coherence time. Therefore, we develop a method for estimating the acceleration parameter using the updated state vectors.

We define the long-term state transition equation, which states the relationship between the initial state vector \mathbf{t}_0 and the current state vector \mathbf{t}_ℓ at time ℓ , such that

$$\begin{aligned}
\mathbf{t}_\ell &= \mathbf{A}^\ell \mathbf{t}_0 + \sum_{\tau=1}^{\ell} \mathbf{A}^{\tau-1} \mathbf{b} \alpha + \sum_{\tau=1}^{\ell} \mathbf{A}^{\tau-1} \mathbf{c}_{\tau-1} \\
&= \mathbf{A}^\ell \mathbf{t}_0 + \tilde{\mathbf{b}}_\ell \alpha + \tilde{\mathbf{c}}_\ell,
\end{aligned} \quad (13)$$

where the modified acceleration transition vector is given by $\tilde{\mathbf{b}}_\ell \doteq \sum_{\tau=1}^{\ell} \mathbf{A}^{\tau-1} \mathbf{b} = [(\ell T_s)^2/2 \cos \varphi, (\ell T_s)^2/2 \sin \varphi, \ell T_s]^T$, and the modified error vector is $\tilde{\mathbf{c}}_\ell \doteq \sum_{\tau=1}^{\ell} \mathbf{A}^{\tau-1} \mathbf{c}_{\tau-1}$.

The state vector can be modeled using the estimated state vector and its corresponding covariance matrix, such as

$$\mathbf{t}_\ell = \hat{\mathbf{t}}_\ell + \mathbf{e}_\ell, \quad (14)$$

where the error term is modeled based on the *Correlated Grassmannian* algorithm such as $\mathbf{e}_\ell \doteq \mathbf{Q}_\ell^{\frac{1}{2}} \mathbf{w} / \|\mathbf{Q}_\ell^{\frac{1}{2}} \mathbf{w}\|_2$ with a random vector $\mathbf{w} \sim \mathcal{N}(\mathbf{0}_3, \mathbf{I}_3)$. By substituting the vector in (14) into state equation (13), we rewrite the state model in (13) for the acceleration parameter estimation such that

$$\tilde{\mathbf{t}}_\ell \doteq \hat{\mathbf{t}}_\ell - \mathbf{A}^\ell \mathbf{t}_0 = \tilde{\mathbf{b}}_\ell \alpha + \tilde{\mathbf{c}}_\ell - \mathbf{e}_\ell,$$

where the error vector can be modeled using a normal distribution, such that $\tilde{\mathbf{c}}_\ell \sim \mathcal{N}(\mathbf{0}_3, \mathbf{C}_\ell)$. The covariance matrix is derived as

$$\mathbf{C}_\ell \doteq \mathbb{E}[\tilde{\mathbf{c}}_\ell \tilde{\mathbf{c}}_\ell^T] = \sum_{\tau=1}^{\ell} \mathbf{A}^{\tau-1} \mathbf{Q}_\omega (\mathbf{A}^{\tau-1})^T \in \mathbb{R}^{3 \times 3}.$$

Based on the minimum variance unbiased (MVU) estimator in [21], the acceleration parameter is estimated as

$$\hat{\alpha} = \frac{\tilde{\mathbf{b}}_\ell^T (\mathbf{C}_\ell + \mathbf{Q}_\ell)^{-1} \tilde{\mathbf{t}}_\ell}{\tilde{\mathbf{b}}_\ell^T (\mathbf{C}_\ell + \mathbf{Q}_\ell)^{-1} \tilde{\mathbf{b}}_\ell} = \alpha + \frac{\tilde{\mathbf{b}}_\ell^T (\mathbf{C}_\ell + \mathbf{Q}_\ell)^{-1} (\tilde{\mathbf{c}}_\ell - \mathbf{e}_\ell)}{\tilde{\mathbf{b}}_\ell^T (\mathbf{C}_\ell + \mathbf{Q}_\ell)^{-1} \tilde{\mathbf{b}}_\ell}. \quad (15)$$

We also study the performance of the MVU estimator. For any unbiased estimator $\check{\alpha}$, the variance is lower-bounded such that

$$\begin{aligned}
\text{var}(\check{\alpha}) &\geq \left(\mathbb{E} \left[-\frac{\partial^2}{\partial \alpha^2} \ln(p(\tilde{\mathbf{t}}_\ell; \alpha)) \right] \right)^{-1} \\
&= \left(\mathbb{E} \left[\frac{\partial^2}{\partial \alpha^2} \left[\frac{(\tilde{\mathbf{t}}_\ell - \tilde{\mathbf{b}}_\ell \alpha)^T (\mathbf{C}_\ell + \mathbf{Q}_\ell)^{-1} (\tilde{\mathbf{t}}_\ell - \tilde{\mathbf{b}}_\ell \alpha)}{2} \right. \right. \right. \\
&\quad \left. \left. \left. + \ln(2\pi|\mathbf{C}_\ell + \mathbf{Q}_\ell|) \right] \right] \right)^{-1} \\
&= \left(\mathbb{E} \left[\frac{\partial}{\partial \alpha} \left[\tilde{\mathbf{b}}_\ell^T (\mathbf{C}_\ell + \mathbf{Q}_\ell)^{-1} \tilde{\mathbf{t}}_\ell \right. \right. \right. \\
&\quad \left. \left. \left. + \alpha (\tilde{\mathbf{b}}_\ell^T (\mathbf{C}_\ell + \mathbf{Q}_\ell)^{-1} \tilde{\mathbf{b}}_\ell) \right] \right] \right)^{-1} \\
&= (\tilde{\mathbf{b}}_\ell^T (\mathbf{C}_\ell + \mathbf{Q}_\ell)^{-1} \tilde{\mathbf{b}}_\ell)^{-1} = 1/I(\alpha)
\end{aligned}$$

where $\tilde{\mathbf{t}}_\ell \sim \mathcal{N}(\tilde{\mathbf{b}}_\ell \alpha, \mathbf{C}_\ell + \mathbf{Q}_\ell)$, $I(\alpha)$ is the Fisher information, and the Cramer-Rao lower bound (CRLB) is given by $1/I(\alpha)$.

Algorithm 1 State tracking algorithm using the EKF algorithm

Initialization

- 1: Initial state vector, $\mathbf{t}_0 = [x_0, y_0, v_0]^T$, $\hat{\mathbf{t}}_0 = \mathbf{t}_0 + \mathbf{e}_\epsilon$
- 2: Initial covariance matrix, $\mathbf{Q}_0 = \sigma_\epsilon^2 (\mathbf{t}_0 \mathbf{t}_0^T)$

Linear state prediction

- 3: Predict state vector
 $\hat{\mathbf{t}}_{\ell|\ell-1} = \hat{\mathbf{A}}\hat{\mathbf{t}}_{\ell-1}$, w/o estimated $\hat{\alpha}$
 $\hat{\mathbf{t}}_{\ell|\ell-1} = \hat{\mathbf{A}}\hat{\mathbf{t}}_{\ell-1} + \mathbf{b}\hat{\alpha}$, w/ estimated $\hat{\alpha}$
- 4: Update covariance matrix
 $\mathbf{Q}_{\ell|\ell-1} = \mathbf{A}\mathbf{Q}_{\ell-1}\mathbf{A}^T + \mathbf{Q}_\alpha + \mathbf{Q}_\omega$, w/o estimated $\hat{\alpha}$
 $\mathbf{Q}_{\ell|\ell-1} = \mathbf{A}\mathbf{Q}_{\ell-1}\mathbf{A}^T + \mathbf{Q}_\omega$, w/ estimated $\hat{\alpha}$

Uplink channel sounding

- 5: Compute combiner at RSU
 $\mathbf{z}_\ell = \mathbf{v} \left\{ \left(\mathbf{D}_{\ell|\ell-1} \mathbf{Q}_{\ell|\ell-1} \mathbf{D}_{\ell|\ell-1}^H + \frac{\mathbf{I}_M}{\rho_e} \right)^{-1} \left(\mathbf{D}_{\ell|\ell-1} \mathbf{Q}_{\ell|\ell-1}^2 \mathbf{D}_{\ell|\ell-1}^H \right) \right\}$
- 6: Conduct uplink channel sounding
 $r_\ell = \mathbf{z}_\ell \mathbf{h}(\psi_\ell) + n_\ell \rightarrow \tilde{\mathbf{r}}_\ell = \tilde{\mathbf{Z}}_\ell \tilde{\mathbf{h}}(\psi_\ell) + \tilde{n}_\ell$

State update based on uplink channel sounding

- 7: Design Kalman gain matrix
 $\tilde{\mathbf{K}}_\ell = \mathbf{Q}_{\ell|\ell-1} \tilde{\mathbf{D}}_{\ell|\ell-1}^T \tilde{\mathbf{Z}}_\ell^T$
 $\left(\tilde{\mathbf{Z}}_\ell \tilde{\mathbf{D}}_{\ell|\ell-1} \mathbf{Q}_{\ell|\ell-1} \tilde{\mathbf{D}}_{\ell|\ell-1}^T \tilde{\mathbf{Z}}_\ell^T + \frac{\mathbf{I}_2}{2\rho_e} \right)^{-1}$
- 8: Update state vector
 $\hat{\mathbf{t}}_\ell = \hat{\mathbf{t}}_{\ell|\ell-1} + \tilde{\mathbf{K}}_\ell (\tilde{\mathbf{r}}_\ell - \tilde{\mathbf{Z}}_\ell \tilde{\mathbf{h}}(\mathbf{g}(\hat{\mathbf{t}}_{\ell|\ell-1})))$
- 9: Update covariance matrix
 $\mathbf{Q}_\ell = (\mathbf{I}_3 - \tilde{\mathbf{K}}_\ell \tilde{\mathbf{Z}}_\ell \tilde{\mathbf{D}}_{\ell|\ell-1}) \mathbf{Q}_{\ell|\ell-1}$

The variance of the MVU estimator in (15) is calculated as

$$\begin{aligned} \text{var}(\hat{\alpha}) &= \mathbb{E}[(\hat{\alpha} - \mathbb{E}[\hat{\alpha}])(\hat{\alpha} - \mathbb{E}[\hat{\alpha}])^T] \\ &\stackrel{(a)}{=} \mathbb{E}[(\hat{\alpha} - \alpha)(\hat{\alpha} - \alpha)^T] \\ &= \mathbb{E}\left[\frac{\tilde{\mathbf{b}}_\ell^T (\mathbf{C}_\ell + \mathbf{Q}_\ell)^{-1} (\tilde{\mathbf{c}}_\ell - \mathbf{e}_\ell) (\tilde{\mathbf{c}}_\ell - \mathbf{e}_\ell)^T (\mathbf{C}_\ell + \mathbf{Q}_\ell)^{-1} \tilde{\mathbf{b}}_\ell}{|\tilde{\mathbf{b}}_\ell^T (\mathbf{C}_\ell + \mathbf{Q}_\ell)^{-1} \tilde{\mathbf{b}}_\ell|^2}\right] \\ &\stackrel{(b)}{=} \frac{\tilde{\mathbf{b}}_\ell^T (\mathbf{C}_\ell + \mathbf{Q}_\ell)^{-1} \mathbb{E}[(\tilde{\mathbf{c}}_\ell - \mathbf{e}_\ell)(\tilde{\mathbf{c}}_\ell - \mathbf{e}_\ell)^T] (\mathbf{C}_\ell + \mathbf{Q}_\ell)^{-1} \tilde{\mathbf{b}}_\ell}{|\tilde{\mathbf{b}}_\ell^T (\mathbf{C}_\ell + \mathbf{Q}_\ell)^{-1} \tilde{\mathbf{b}}_\ell|^2} \\ &\stackrel{(c)}{=} (\tilde{\mathbf{b}}_\ell^T (\mathbf{C}_\ell + \mathbf{Q}_\ell)^{-1} \tilde{\mathbf{b}}_\ell)^{-1} \end{aligned}$$

where (a) is derived based on the unbiased estimator, (b) is derived because only $\tilde{\mathbf{c}}_\ell$ and \mathbf{e}_ℓ are random variables, and (c) is derived because $\mathbb{E}[\tilde{\mathbf{c}}_\ell \tilde{\mathbf{c}}_\ell^T] = \mathbf{C}_\ell$, $\mathbb{E}[\mathbf{e}_\ell \mathbf{e}_\ell^T] = \mathbf{Q}_\ell$, and $\mathbb{E}[\tilde{\mathbf{c}}_\ell \mathbf{e}_\ell^T] = \mathbf{0}_{3 \times 3}$. The variance of $\hat{\alpha}$ is equal to or greater than the CRLB, which denotes the variance of the proposed estimator, such that $\text{var}(\hat{\alpha}) \geq 1/\text{I}(\alpha) = \text{var}(\hat{\alpha})$. We conclude that the MVU estimator in (15) is efficient because it achieves the CRLB.

Assuming that the acceleration parameter is properly estimated, we can reduce the randomness/uncertainty in the state prediction process.² In the proposed EKF algorithm, we focus on correcting the position and velocity changes due to the error parameter, without needing to consider the changes due to the acceleration of the vehicle, α . In the state prediction process,

²The estimated acceleration parameter, $\hat{\alpha}$, applies to the state prediction process only when the difference between the previous and current estimations is not greater than the predefined threshold parameter, α_{thres} .

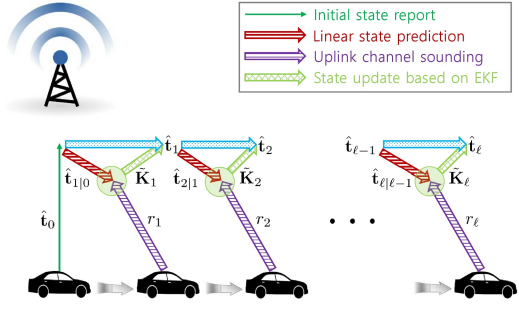


Fig. 2. State tracking algorithm with extended Kalman filter.

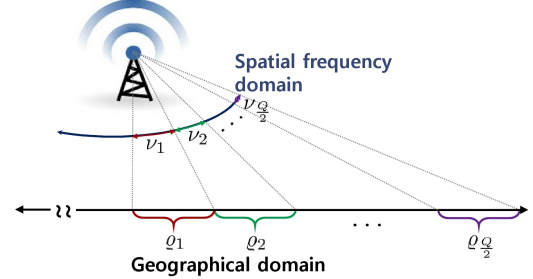


Fig. 3. Sub-range transformation between the geographical domain and the spatial frequency domain.

the state vector and corresponding covariance matrix can be predicted as

$$\begin{aligned} \hat{\mathbf{t}}_{\ell|\ell-1} &= \hat{\mathbf{A}}\hat{\mathbf{t}}_{\ell-1} + \mathbf{b}\hat{\alpha}, \\ \mathbf{Q}_{\ell|\ell-1} &= \mathbf{A}\mathbf{Q}_{\ell-1}\mathbf{A}^T + \mathbf{Q}_\omega. \end{aligned}$$

The transmit combiner for the uplink sounding process can be designed to cover a narrower beam width area, because we only consider the covariance matrix due to the error parameter. Finally, the EKF algorithm for the state update process is summarized in Algorithm 1 and depicted in Fig. 2.

IV. DOWNLINK BEAMFORMER DESIGN ALGORITHM

We design a beamforming codebook by exploiting the knowledge of road structures. Furthermore, we develop a codeword selection algorithm to obtain a robust beamformer based on the predicted channel information. Typically, each beamforming codeword covers a certain beam-region in the spatial frequency domain, which maps onto a geographic area. The conventional beamformer is designed to generate a beam pattern (BP) within an equally-spaced beam-region [34]–[36]. Assuming there are Q codewords $\{\mathbf{u}_1, \dots, \mathbf{u}_Q\}$ in the codebook, each beam-region is defined to have the same length, $|\tilde{\nu}| = \frac{\nu^{\text{ub}} - \nu^{\text{lb}}}{Q} = \frac{2\nu^{\text{ub}}}{Q}$, in the spatial frequency domain, where $(\nu^{\text{lb}}, \nu^{\text{ub}})$ denotes the left-hand/right-hand edges of the entire beam-region, respectively.

However, the conventional beam-region division approach may not be effective in V2I communications because the distance between RSU and the vehicle on the y -axis, $k = \sqrt{y^2 + h^2}$, is significantly shorter than the length of the road on the x -axis. As shown in Fig. 3, the difference between the beam width in the spatial frequency domain and the projected length on the road in the geographical domain varies depending

on the vehicle location. The beamforming codewords need to be designed by taking the distortion of the projection into account.

1) *Beam-region division algorithm*: The studies in this sub-section are aimed at defining the target beam-region of interest for each beamforming codeword. For a simple analysis, the position on the y -axis is assumed to have a fixed value.³ In the geographical domain, the q -th sub-range is defined by $\varrho_q \doteq [\varrho_q^{\text{lb}}, \varrho_q^{\text{ub}}]$, where ϱ_q^{lb} and ϱ_q^{ub} denote the left-hand edge and the right-hand edge of the sub-range, respectively. We also denote $\nu_q \doteq [\nu_q^{\text{lb}}, \nu_q^{\text{ub}}]$ as the q -th beam-region in the spatial frequency domain, where ν_q^{lb} and ν_q^{ub} are the left-hand/right-hand edges of the beam-region, respectively. The geographic sub-range can be converted into the beam-region ($\nu_q \doteq D[\varrho_q]$) and vice versa ($\varrho_q \doteq D^{-1}[\nu_q]$). For the remainder of this sub-section, we only consider the positive region, because the opposite region can be expressed by using symmetry.

Before developing the beam-region-division algorithm, we pause to catch up on the conversion process between the geographical and spatial frequency domains. For further discussion, each geographic sub-range is tentatively defined as having the same length, $|\tilde{\varrho}| = \frac{\varrho^{\text{ub}} - \varrho^{\text{lb}}}{Q} = \frac{2\varrho^{\text{ub}}}{Q}$, where $(\varrho^{\text{lb}}, \varrho^{\text{ub}})$ denotes the left-hand/right-hand edges, respectively, of the geographic range. This means that all geographic sub-ranges are the same: $|\tilde{\varrho}| = |\varrho_q|$ for all $q \in \{1, \dots, Q\}$. In the spatial frequency domain, however, the transformed beam-region, $\nu_q \doteq D[\varrho_q]$ varies due to nonlinear transformation.

We study the change in the transformed beam-region in the spatial frequency domain. First, we verify that the beam-region, ν_q , strictly decreases for q , because the difference between the derivative of the beam-regions is derived as

$$\begin{aligned} \dot{T}(\varrho_q^{\text{ub}}, y) - \dot{T}(\varrho_q^{\text{lb}}, y) &= \frac{\pi k^2}{(k^2 + (\varrho_q^{\text{ub}})^2)^{\frac{3}{2}}} - \frac{\pi k^2}{(k^2 + (\varrho_q^{\text{lb}})^2)^{\frac{3}{2}}} \\ &\stackrel{(a)}{<} 0, \end{aligned}$$

where the nonlinear transformation function, $T(\cdot)$, is defined in (2), $k = \sqrt{y^2 + h^2}$, and (a) holds with $(k^2 + (\varrho_q^{\text{ub}})^2)^{\frac{3}{2}} > (k^2 + (\varrho_q^{\text{lb}})^2)^{\frac{3}{2}}$ because $(\cdot)^{\frac{3}{2}}$ is a strictly increasing function, and $\varrho_q^{\text{ub}} > \varrho_q^{\text{lb}}$.

Further, we take a closer look at the beam-regions as a function of the position on the road. The length of the first beam-region in the spatial frequency domain is greater than that of the equally divided beam-region, such that $|\nu_1| > |\tilde{\nu}|$, because

$$\begin{aligned} |\nu_1| - |\tilde{\nu}| &\stackrel{(a)}{=} T(\varrho_1^{\text{ub}}, y) - 2T(\varrho^{\text{ub}}, y)Q^{-1} \\ &\stackrel{(b)}{=} \frac{\pi|\tilde{\varrho}|}{(k^2 + |\tilde{\varrho}|^2)^{\frac{1}{2}}} - \frac{\pi|\tilde{\varrho}|}{(k^2 + (|\tilde{\varrho}|Q/2)^2)^{\frac{1}{2}}} \stackrel{(c)}{>} 0, \end{aligned}$$

where (a) holds because $|\tilde{\nu}| = 2\nu^{\text{ub}}/Q$, (b) holds with $\varrho^{\text{ub}} = |\tilde{\varrho}|Q/2$, and (c) holds because $(\cdot)^{\frac{1}{2}}$ is a strictly increasing function with $Q > 2$. Furthermore, assuming that the vehicle is far away from the central location on the road, the length of the converted beam-region is compared to that of the equally divided beam-region in the following Lemma.

³Since we assume that the vehicle does not change lanes, the change of position on the y -axis is negligible compared to that on the x -axis.

Lemma 1: Assuming $|x| \gg k$, the length of the equally divided beam-region over the length of the converted beam-region is greater than one, such that $|\tilde{\nu}|/|\nu_q| > 1$ when the approximated condition, $|x| > \frac{\sqrt{|\varrho|(|\varrho| + rQ)}}{2}$, holds.

Proof: The ratio between the length of the equally divided beam-region and the length of the converted beam-region is approximated by

$$\begin{aligned} \Delta_q &\doteq \frac{|\tilde{\nu}|}{|\nu_q|} = \frac{2\pi Q^{-1} \left(1 + \left(\frac{2k}{|\tilde{\varrho}|Q}\right)^2\right)^{-\frac{1}{2}}}{\pi \left(1 + \left(\frac{k}{\varrho_q^{\text{ub}}}\right)^2\right)^{-\frac{1}{2}} - \pi \left(1 + \left(\frac{k}{\varrho_q^{\text{lb}}}\right)^2\right)^{-\frac{1}{2}}} \\ &\stackrel{(a)}{\approx} \frac{2\pi Q^{-1} \left(1 - \frac{k}{|\tilde{\varrho}|Q}\right)}{\pi \left(1 - \frac{k}{2\varrho_q^{\text{ub}}}\right) - \pi \left(1 - \frac{k}{2\varrho_q^{\text{lb}}}\right)} = \frac{\varrho_q^{\text{ub}} \varrho_q^{\text{lb}} (|\tilde{\varrho}|Q - k)}{r(|\tilde{\varrho}|Q/2)^2}, \end{aligned}$$

where (a) is approximated because $(1 + \zeta^2)^{-\frac{1}{2}} \simeq (1 - \frac{1}{2}\zeta)$ for a sufficiently small ζ based on the assumption $|x| \gg k$. The ratio is greater than one when the condition $\frac{\varrho_q^{\text{ub}} \varrho_q^{\text{lb}} (|\tilde{\varrho}|Q - k)}{k(|\tilde{\varrho}|Q/2)^2} > 1$ holds. Note that this condition has been rewritten as $\varrho_q^{\text{ub}} \varrho_q^{\text{lb}} > \frac{k(|\tilde{\varrho}|Q/2)^2}{|\tilde{\varrho}|Q - k}$. Assuming that the left-hand/right-hand edges of the sub-range are defined as a function of the position parameter, such that $\{\varrho_q^{\text{lb}}, \varrho_q^{\text{ub}}\} \doteq \{p - \frac{|\tilde{\varrho}|}{2}, p + \frac{|\tilde{\varrho}|}{2}\}$, the condition can be approximated as

$$|x| > \sqrt{\frac{|\tilde{\varrho}|^2}{4} + \frac{k(|\tilde{\varrho}|Q/2)^2}{|\tilde{\varrho}|Q - k}} \stackrel{(a)}{\approx} \frac{\sqrt{|\varrho|(|\varrho| + rQ)}}{2},$$

where the approximation in (a) holds with $|\tilde{\varrho}|Q - k \simeq |\tilde{\varrho}|Q$ because $|\varrho|Q \gg k$. ■

Based on Parseval's theorem [37], the total amount of energy with respect to the BP over the entire beam-region is fixed to the finite value $\frac{2\pi}{M}$. In previous studies assuming a uniformly distributed beam direction, the length of each beam-region is evenly divided to uniformly split the energy over the spatial frequency domain [34]–[36]. However, it is not reasonable to assume that the directions of a dominant radio path are uniformly distributed, because wireless coverage in a V2I network is very different from that in conventional cellular networks. Assuming a uniform distribution of vehicles on the road, the beamforming gain must be uniformly distributed over the entire geographic range to maximize the average data-rate.

Around the center of the road, e.g., $|x| < k$, it is effective to equally divide the geographic sub-range. However, as discussed in Lemma 1, the beam width of the converted beam-region becomes narrower than that of the equally divided beam-region, $|\tilde{\nu}|$, when the vehicle moves toward the road edge. If the beam width of the converted beam-region is smaller than $\frac{2\pi}{M}$, then the total amount of energy, $\frac{2\pi}{M}$, cannot be contained within the beam-region because the maximum value of the normalized BP is limited to one. For this reason, an oversampling effect occurs because neighboring codewords generate overlapped beam patterns. As the vehicle drives to the edge in the geographical domain, the oversampling effect becomes severe because too many beamformers point in a similar direction, which is the end of the spatial frequency domain. To compensate for the extreme oversampling effect, we impose a minimum constraint on the beam width of a codeword.

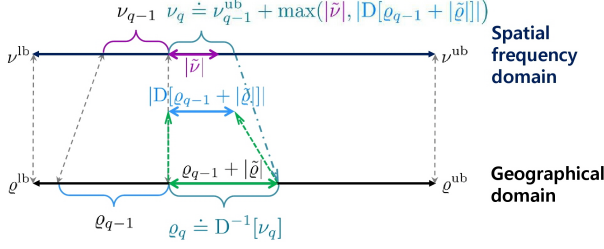


Fig. 4. Proposed sub-range partitioning algorithm.

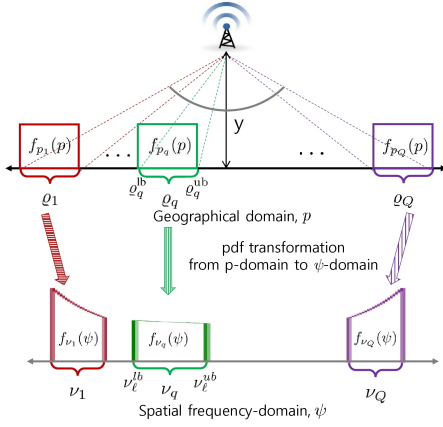


Fig. 5. Domain transformation for beamformer codebook design.

A beam-region-division algorithm is proposed to resolve the overlapping BP problem. First, the equally spaced geographic sub-range, $\rho_{q-1} + |\tilde{\rho}|$, is defined as the sub-range candidate. The sub-range candidate is then converted into the spatial frequency domain, such that $D[\rho_{q-1} + |\tilde{\rho}|]$, as depicted in Fig. 4. If the length of the converted beam-region is greater than that of the equally spaced beam-region $|\tilde{\nu}|$, then the sub-range candidate chosen will be the q -th sub-range. To avoid an overlapping BP scenario, however, if the length of the converted beam-region is smaller than $|\tilde{\nu}|$, then the q -th beam-region will be designed to have a predefined minimum length $|\tilde{\nu}|$ in the spatial frequency domain. Based on the beam-region division algorithm, the beam-region and geographic sub-range are defined as $\{\nu_q, \rho_q\} \doteq \{\nu_{q-1}^{\text{ub}} + \max(|\tilde{\nu}|, |D[\rho_{q-1} + |\tilde{\rho}|]|), D^{-1}[\nu_q]\}$. If both the geographical and spatial frequency domains are initially divided by Q , such that $\{|\tilde{\nu}|, |\tilde{\rho}|\} = \{\frac{2\nu^{\text{ub}}}{Q}, \frac{2\rho^{\text{ub}}}{Q}\}$, then the total number of beam-regions that are divided based on the proposed algorithm, will be less than the predefined number of codewords, Q . For this reason, both domains will be divided into more pieces than Q until the set of Q beam-regions is constructed.

2) *Codebook design for downlink beamforming:* We design the transmit beamformer based on predefined geographic sub-ranges and beam-regions. In the previous sub-section, the entire geographic range is divided into Q non-overlapping sub-ranges⁴, such that $\{\rho_1, \dots, \rho_Q\}$. In this paper, we focus on designing a transmit beamformer that generates a favorable BP in each target geographic range.

⁴After completing the beam-region-division algorithm, the index restarts at 1 including negative beam-regions.

Assuming that the positions of vehicles follow a uniform distribution along the road, the probability density function (pdf) of the position variable in ρ_q can be modeled by

$$f_{\rho_q}(x) = \frac{u(x - \rho_q^{\text{lb}}) - u(x - \rho_q^{\text{ub}})}{\rho_q^{\text{ub}} - \rho_q^{\text{lb}}}.$$

In the geographical domain, the BP should be uniformly distributed because the data-rate is computed with respect to the uniformly distributed vehicle positions on the road.

The position variable x can be written as a function of spatial frequency ψ , such that $x = k\psi(\pi^2 - \psi^2)^{-\frac{1}{2}}$, as in (2). Therefore, as depicted in Fig. 5, the pdf in the geographical spatial frequency domain can be transformed into the spatial frequency domain, such as

$$\begin{aligned} f_{\nu_q}(\psi) &= f_{\rho_q}(k\psi(\pi^2 - \psi^2)^{-\frac{1}{2}}) \left| \frac{d}{d\psi} (k\psi(\pi^2 - \psi^2)^{-\frac{1}{2}}) \right| \\ &= \frac{|\pi^2 k(\pi^2 - \psi^2)^{-3/2}|}{\rho_q^{\text{ub}} - \rho_q^{\text{lb}}} \left[u(k\psi(\pi^2 - \psi^2)^{-\frac{1}{2}} - \rho_q^{\text{lb}}) \right. \\ &\quad \left. - u(k\psi(\pi^2 - \psi^2)^{-\frac{1}{2}} - \rho_q^{\text{ub}}) \right]. \end{aligned} \quad (16)$$

We design the beamforming codeword in order to generate a BP, which is similar to the pdf of the beam direction $f_{\nu_q}(\psi)$ in the spatial frequency domain. The optimal BP of the q -th codeword is defined as

$$\begin{aligned} G_q^{\text{opt}}(\psi) &= \chi f_{\nu_q}(\psi) \\ &\stackrel{(a)}{=} \frac{2\pi |\pi^2 k(\pi^2 - \psi^2)^{-3/2}|}{M(\rho_q^{\text{ub}} - \rho_q^{\text{lb}})} \left[u(k\psi(\pi^2 - \psi^2)^{-\frac{1}{2}} - \rho_q^{\text{lb}}) \right. \\ &\quad \left. - u(k\psi(\pi^2 - \psi^2)^{-\frac{1}{2}} - \rho_q^{\text{ub}}) \right], \end{aligned} \quad (17)$$

where χ is the scaling constant. All BPs satisfy the integral constraint, $\int_{-\pi}^{\pi} G_q^{\text{opt}}(\psi) d\psi = \frac{2\pi}{M}$, based on Parseval's theorem [37]. The scaling coefficient in (a) is thus computed as $\chi = \frac{2\pi}{M}$, as in [35]. Notably, beamforming gain is upper bounded by the unit gain.

We focus on minimizing the mean squared error between the optimal BP and the actual BP to compute the beamforming codeword. Similar to [34], [35], we construct the beamformer, $\mathbf{u}_q = \mathbf{F}_q \mathbf{v}_q$, such that

$$(\mathbf{F}_q, \mathbf{v}_q) = \arg \min_{\tilde{\mathbf{F}}, \tilde{\mathbf{v}}} \int_{-\pi}^{\pi} \left| G_q^{\text{opt}}(\psi) - |\mathbf{d}_M^H(\psi) \tilde{\mathbf{F}} \tilde{\mathbf{v}}|^2 \right|^2 d\psi. \quad (18)$$

The beamformer that minimizes the mean squared error in (18) is chosen from among the beamformer candidates, as in [38]. Please see [38] for more details on the method of generating beamformer candidates, and for the final codeword selection process.

Finally, the beamforming codebook, which consists of Q predefined codewords, is constructed as $\mathcal{U}_Q^{\text{BF}} \doteq \{\mathbf{u}_1, \dots, \mathbf{u}_Q\}$. Example BPs of beamforming codewords and codebook are depicted in Figs. 6 and 7, respectively. The dotted lines represent the ideal BP in (17), and the solid lines represent the actual BP, generated by $\mathbf{u}_q = \mathbf{F}_q \mathbf{v}_q$ in (18). Fig. 6 shows that the beamformer design algorithm in [38] is effective at generating a BP that is similar to the ideal BP in (17).

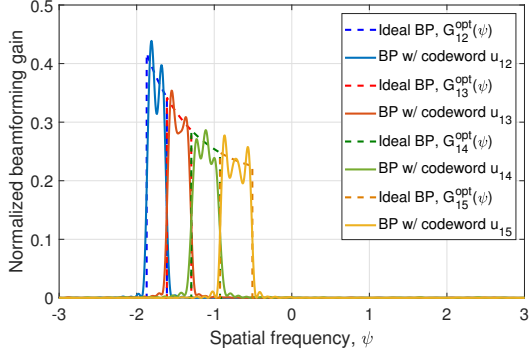


Fig. 6. Comparison between ideal and actual beam patterns with beamforming codebook with $Q = 32$ codewords and $M = 64$ transmit antennas.

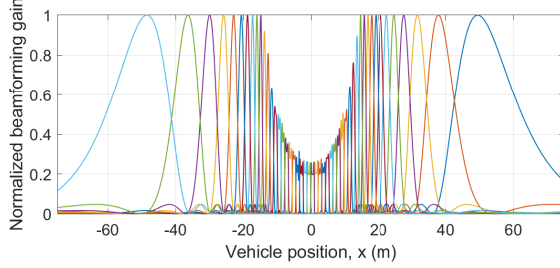


Fig. 7. BP example of $Q = 48$ codewords in the codebook \mathcal{U}_{48}^{BF} and $M = 96$ transmit antennas ($y = 8.5$ m).

3) *Beamformer selection algorithm*: The transmit beamformer should be chosen for a given set of state vectors $\hat{\mathbf{t}}_\tau$ and covariance matrices \mathbf{Q}_τ at time τ . Note that τ is the beamformer switching time, which is a nonnegative multiple of the channel sounding period T_s . Although uplink sounding is conducted for every T_s , it is not practical to recompute the transmit beamformer frequently. The transmit beamformer, \mathbf{c}_τ , is periodically designed every $T_d = \Omega T_s$ seconds. The beamformer \mathbf{c}_τ at time instance τ should be chosen to provide mobile service with a large beamforming gain within the next period, i.e., $\{(\tau + 1), \dots, (\tau + \Omega)\}$.

First, we estimate the future state vectors without the aid of uplink sounding. The estimated state vectors are denoted by $\{\tilde{\mathbf{t}}_{\tau+1}, \dots, \tilde{\mathbf{t}}_{\tau+\Omega}\}$. Without the state update process based on the uplink sounding observations, the predicted state vector and covariance matrix cannot be corrected using the Kalman gain matrix in (10). Therefore, the transmit beamformer for the next T_d seconds has to be designed using the state vectors and covariance matrices that are estimated based only on the state prediction process. For a given estimated state vector $\hat{\mathbf{t}}_\tau$ at time instance τ , the state vectors are predicted as

$$\begin{aligned}\tilde{\mathbf{t}}_{\tau+t} &= \mathbf{A}^t \hat{\mathbf{t}}_\tau, \quad \text{w/o estimated } \hat{\alpha}, \\ \tilde{\mathbf{t}}_{\tau+t} &= \mathbf{A}^t \hat{\mathbf{t}}_\tau + \mathbf{b} \hat{\alpha}, \quad \text{w/ estimated } \hat{\alpha}.\end{aligned}$$

Furthermore, the predicted covariance matrix is predicted as

$$\begin{aligned}\tilde{\mathbf{Q}}_{\tau+t} &= \mathbf{A}^t \mathbf{Q}_\tau (\mathbf{A}^T)^t + \sum_{\tau=0}^{t-1} \mathbf{A}^\tau (\mathbf{Q}_\alpha + \mathbf{Q}_\omega) (\mathbf{A}^T)^\tau, \quad \text{w/o } \hat{\alpha}, \\ \tilde{\mathbf{Q}}_{\tau+t} &= \mathbf{A}^t \mathbf{Q}_\tau (\mathbf{A}^T)^t + \sum_{\tau=0}^{t-1} \mathbf{A}^\tau \mathbf{Q}_\omega (\mathbf{A}^T)^\tau, \quad \text{w/ } \hat{\alpha},\end{aligned}$$

The statistical distribution of the position variable is defined for the given estimated state vector and covariance matrix. In the estimated state vector, the position variable on the x -axis can be modeled by $x_{\tau+t} = \tilde{x}_{\tau+t} + \nu_{\tau+t}$, where $\tilde{x}_{\tau+t} = (\tilde{\mathbf{t}}_{\tau+t})_{1,1}$, $\nu_{\tau+t} \sim \mathcal{N}(0, \sigma_{\tau+t}^2)$, and $\sigma_{\tau+t}^2 = (\tilde{\mathbf{Q}}_{\tau+t})_{1,1}$. The position variable on the y -axis is defined by $y_{\tau+t} = (\tilde{\mathbf{t}}_{\tau+t})_{2,1}$. Furthermore, the beam direction at position $x_{\tau+t}$ can be approximated by

$$\begin{aligned}\psi_{\tau+t} &\simeq q(\tilde{x}_{\tau+t}, y_{\tau+t}) + \frac{\partial q(x, y_{\tau+t})}{\partial x} \Big|_{x=\tilde{x}_{\tau+t}} (x_{\tau+t} - \tilde{x}_{\tau+t}) \\ &= q(\tilde{x}_{\tau+t}, y_{\tau+t}) + \dot{q}(\tilde{x}_{\tau+t}, y_{\tau+t})(x_{\tau+t} - \tilde{x}_{\tau+t}),\end{aligned}$$

where $q(\tilde{x}_{\tau+t}, y_{\tau+t}) \doteq \pi \tilde{x}_{\tau+t} (\tilde{x}_{\tau+t}^2 + y_{\tau+t}^2 + h^2)^{-\frac{1}{2}}$, and $\dot{q}(\tilde{x}_{\tau+t}, y_{\tau+t}) = \pi (y_{\tau+t}^2 + h^2) (\tilde{x}_{\tau+t}^2 + y_{\tau+t}^2 + h^2)^{-\frac{3}{2}}$. The beam direction is then modeled as a normal distribution, $\psi_{\tau+t} \sim \mathcal{N}(q(\tilde{x}_{\tau+t}, y_{\tau+t}), \dot{q}(\tilde{x}_{\tau+t}, y_{\tau+t})^2 \sigma_{\tau+t}^2)$.

Second, we define an ideal BP based on the statistical distribution of the estimated beam directions $\{\psi_{\tau+1}, \dots, \psi_{\tau+\Omega}\}$. We define the BP that maximizes the average beamforming gain within the next T_d seconds. The ideal BP is defined by solving the following problem:

$$\begin{aligned}G_\tau^{\text{ideal}}(\psi) &= \arg \max_{\bar{G}(\psi)} \int_{-\pi}^{\pi} \bar{G}(\psi) \left[\sum_{t=1}^{\Omega} f_{\psi_{\tau+t}}(\psi) \right] d\psi \\ &\stackrel{(a)}{\leq} \left(\int_{-\pi}^{\pi} \bar{G}(\psi)^2 d\psi \right)^{-\frac{1}{2}} \left(\int_{-\pi}^{\pi} \left[\sum_{t=1}^{\Omega} f_{\psi_{\tau+t}}(\psi) \right]^2 d\psi \right)^{-\frac{1}{2}},\end{aligned}$$

where (a) is derived based on the Cauchy-Schwarz-Buniakovsky inequality. The equality in (a) holds when the ideal BP is defined by $G_\tau^{\text{ideal}}(\psi) = \chi \sum_{t=1}^{\Omega} f_{\psi_{\tau+t}}(\psi)$, where $\chi \in \mathbb{R}$ denotes the scaling parameter. Since BP satisfies the constraint, $\int_{-\pi}^{\pi} G_\tau^{\text{ideal}}(\psi) d\psi = \frac{2\pi}{M}$, as in [37], the scaling parameter is computed based on the following equation,

$$\int_{-\pi}^{\pi} G_\tau^{\text{ideal}}(\psi) d\psi = \chi \sum_{t=1}^{\Omega} \int_{-\pi}^{\pi} f_{\psi_{\tau+t}}(\psi) d\psi \stackrel{(a)}{\simeq} \chi \Omega = \frac{2\pi}{M},$$

where (a) holds because $\int_{-\pi}^{\pi} f_{\psi_{\tau+t}}(\psi) d\psi \simeq 1$. The ideal BP is defined by

$$G_\tau^{\text{ideal}}(\psi) = \frac{2\pi}{M\Omega} \sum_{t=1}^{\Omega} f_{\psi_{\tau+t}}(\psi). \quad (19)$$

Finally, we propose a method for choosing the beamformer from the beamforming codebook \mathcal{U}_Q^{BF} . We choose a transmit beamformer that can generate a BP similar to the ideal BP in (19). To effectively compare the beamformer's BP with the ideal BP, each codeword \mathbf{u}_q is mapped to the actual BP vector, $\mathbf{g}_q^{\text{actual}} \in \mathbb{R}^L$, consisting of a finite number of beamforming gain samples. Furthermore, for a given $G_\tau^{\text{ideal}}(\psi)$, we define an ideal BP vector, $\mathbf{g}_\tau^{\text{ideal}} \in \mathbb{R}^L$, consisting of L samples in $G_\tau^{\text{ideal}}(\psi)$. We compare the ideal BP vector, $\mathbf{g}_\tau^{\text{ideal}}$, with the actual BP vectors $\mathbf{g}_q^{\text{actual}}$. The selected transmit beamformer is $\mathbf{c} = \mathbf{u}_{\hat{q}}$, where the selected codeword index is

$$\hat{q} = \arg \max_{q \in \{1, \dots, Q\}} |(\mathbf{g}_\tau^{\text{ideal}})^T \mathbf{g}_q^{\text{actual}}|^2.$$

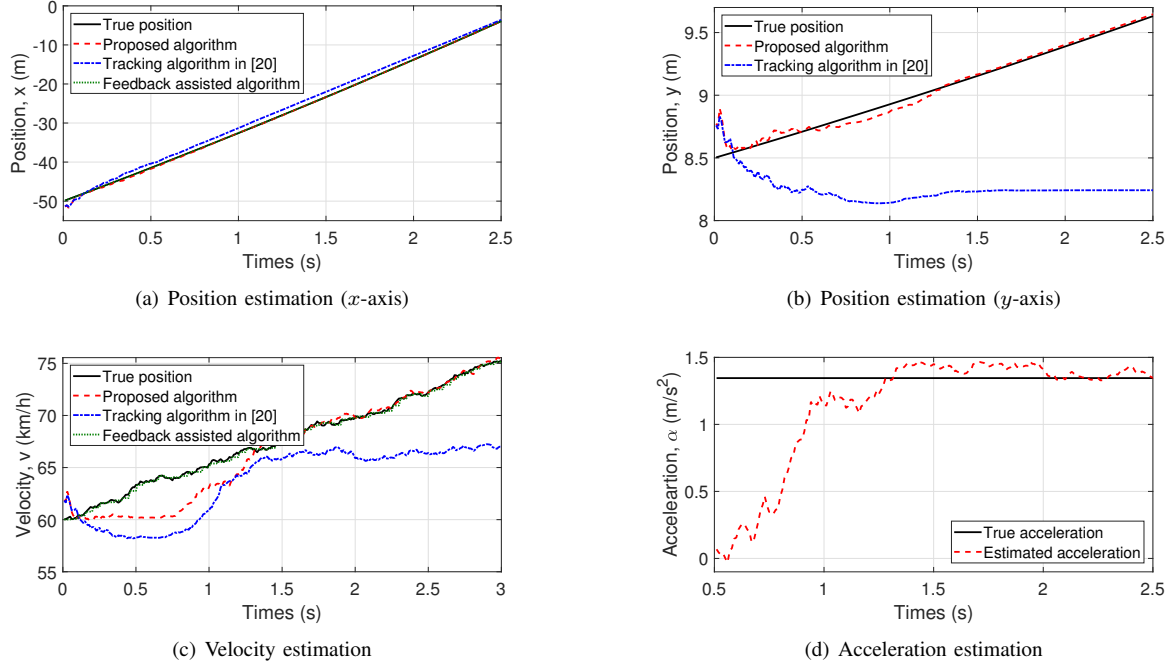


Fig. 8. Examples of state tracking and acceleration estimation algorithms with $M = 128$, $\varrho = -20$ dB, and $\sigma_\epsilon = 10^{-1.5}$.

V. SIMULATION RESULTS

We provide numerical results by evaluating the proposed state tracking algorithm and beamforming codebook design. We consider a hybrid beamforming system using $M = 64, 96$, and 128 transmit antenna elements that are controlled by $N = 4$ radio frequency chains. For Monte-Carlo simulations, we generate $10,000$ independent channels consisting of a line-of-sight and a non-line-of-sight radio path with Rician K -factor of 13 dB. We consider a 20 MHz bandwidth with a center frequency $f_c = 28$ GHz. The noise power integrated over a given bandwidth is $\sigma_n^2 = -174 + 10 \log_{10}(20 \times 10^6) \simeq -101$ dBm and the path-loss exponent is set to $n = 2$. The uplink sounding period is $T_s = 10$ ms, and the downlink transmission period is $T_d = \Omega T_s$ ms, with $\Omega \in \{10, 20\}$.

The height of RSU is $h = 7.5$ m, and the vehicle steering angle is $\varphi = \pi/2^7$. The left-hand edge/right-hand edges of the entire geographic range are defined as $(\varrho^{lb}, \varrho^{ub}) = (-75 \text{ m}, 75 \text{ m})$. In the linear state prediction model, the acceleration parameter is assumed to follow a Gaussian distribution $\alpha \sim \mathcal{N}(0, \sigma_\alpha^2)$ with a standard deviation $\sigma_\alpha = 10^{-1} (v_0 \frac{10^3}{60^2})$ and initial velocity parameter v_0 . Furthermore, the error parameter is assumed to follow a Gaussian distribution with a standard deviation $\sigma_\omega = 10^{-1.5}$. Finally, the threshold for the acceleration estimation process is set to $\alpha_{\text{thres}} = 3\%$.

We evaluate the estimation performance of the proposed vehicle tracking algorithm. We provide examples of state estimation results. For the numerical analysis, the initial state vector is set to $\mathbf{t}_0 = [-50 \text{ m}, 8.5 \text{ m}, 70 \text{ km/h}]^T$. To reflect the initialization error, the feedback error parameter is assumed to follow a Gaussian distribution with a standard deviation $\sigma_\epsilon = 10^{-1.5}$. The state estimation results of the proposed vehicle tracking algorithm are compared with those of the

vehicle tracking algorithm⁵ in [20] and those of the feedback-assisted state tracking approach. In the feedback-assisted state tracking method, the actual state vector is fed back to RSU periodically every $5T_s$, via a feedback link.

As examined in Figs. 8(a) and 8(b), the position variables are well estimated because equation (9), which is used in the state tracking process, is defined as a function of the vehicle position. On the other hand, the velocity estimation illustrated in Fig. 8(c) is relatively worse than the estimation of the position variable because the velocity variable is not directly connected to equation (9) for the state tracking process. Furthermore, due to the initial feedback error, there is a difference between the estimated state vector and true state vector in the initial stage of the tracking process. However, with the uplink channel sounding from the vehicle, the effect of the feedback error can be properly corrected. Hence, the effect of the initial feedback error gradually diminishes as the EKF-based vehicle tracking algorithm progresses. As shown in Figs. 8(a) and 8(c), we performed a comparison with the proposed EKF-based vehicle tracking algorithm and feedback-based tracking method. In the case of the feedback-based tracking algorithm, the vehicle directly transmits the position and velocity information to RSU. Therefore, it can provide a higher estimation performance than the EKF-based algorithm. However, unlike relying upon a sounding signal in the EKF algorithm, the feedback-based algorithm requires additional data transfer fields, which may dramatically increase the payload overhead for the feedback process. Fig. 8(c) shows that the difference between the actual and estimated velocities decreases over time. These results can

⁵The vehicle tracking algorithm in [20] is modified to track the vehicle movement on the x -axis by considering the V2I transmission framework depicted in Fig. 1.

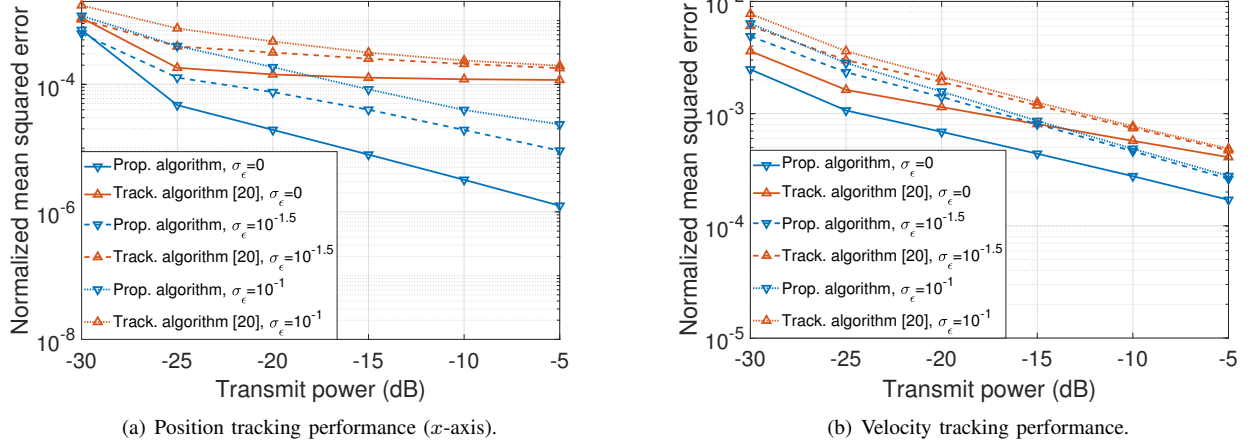


Fig. 9. Normalized mean squared error of vehicle tracking algorithms with $M = 96$ and $\varphi = \pi/2^9$.

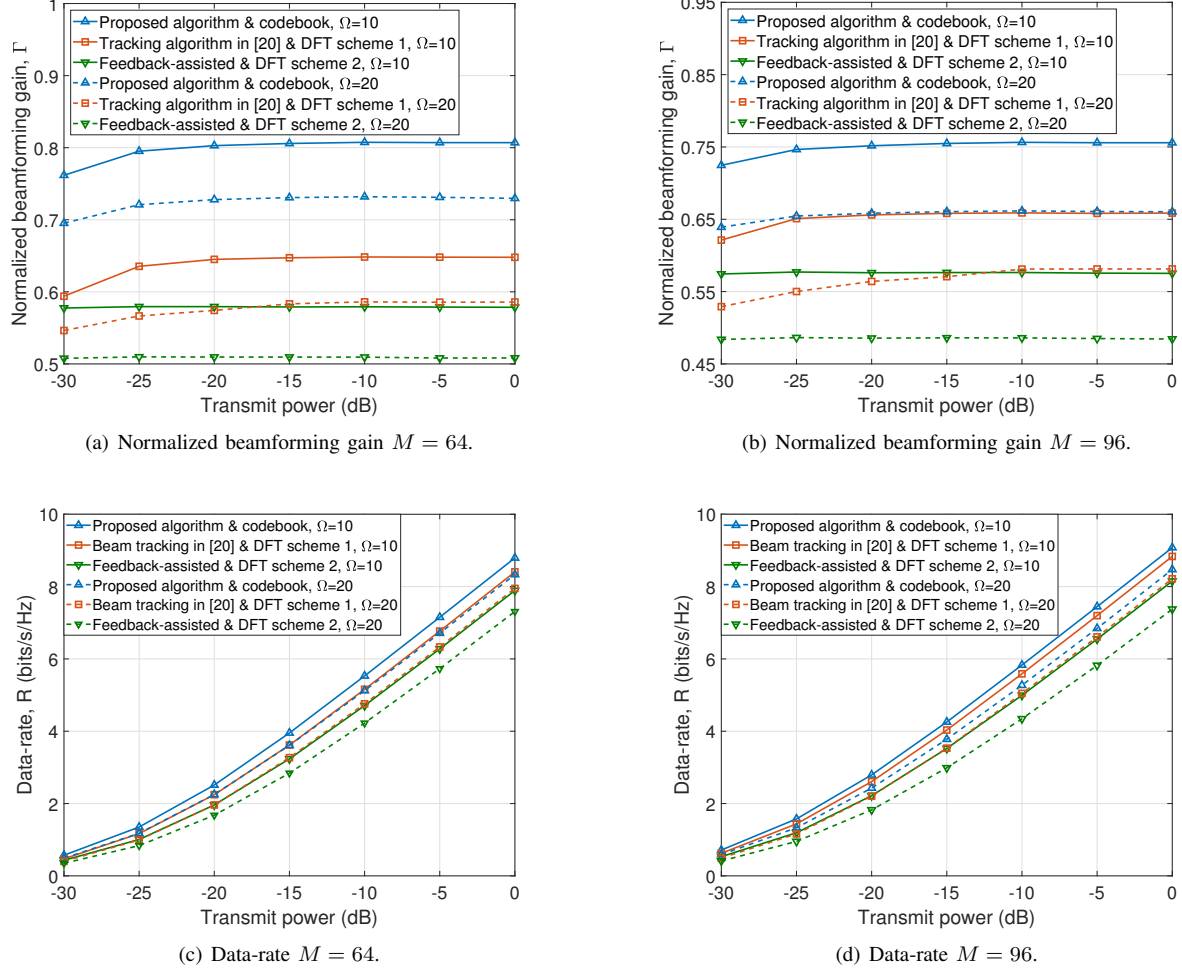


Fig. 10. Beamforming gain and data-rate of single-resolution beamforming codebook ($\Omega = 10, 20$, $Q = Q_1 = M$, $O = 1$, $\sigma_\epsilon = 0$).

be explained by the changes in the acceleration estimation performance depicted in Fig. 8(d). After the proposed acceleration algorithm converges, the estimated acceleration parameter is applied to the state prediction process. Thus, the position and velocity estimation performance improve because RSU can only focus on correcting the error parameter by removing the

acceleration parameter. The state estimation results show that the acceleration estimation will get better as the state tracking performance is enhanced, and vice versa. The state tracking results should be accumulated in order to obtain an estimated acceleration parameter that can be applied to the state tracking process.

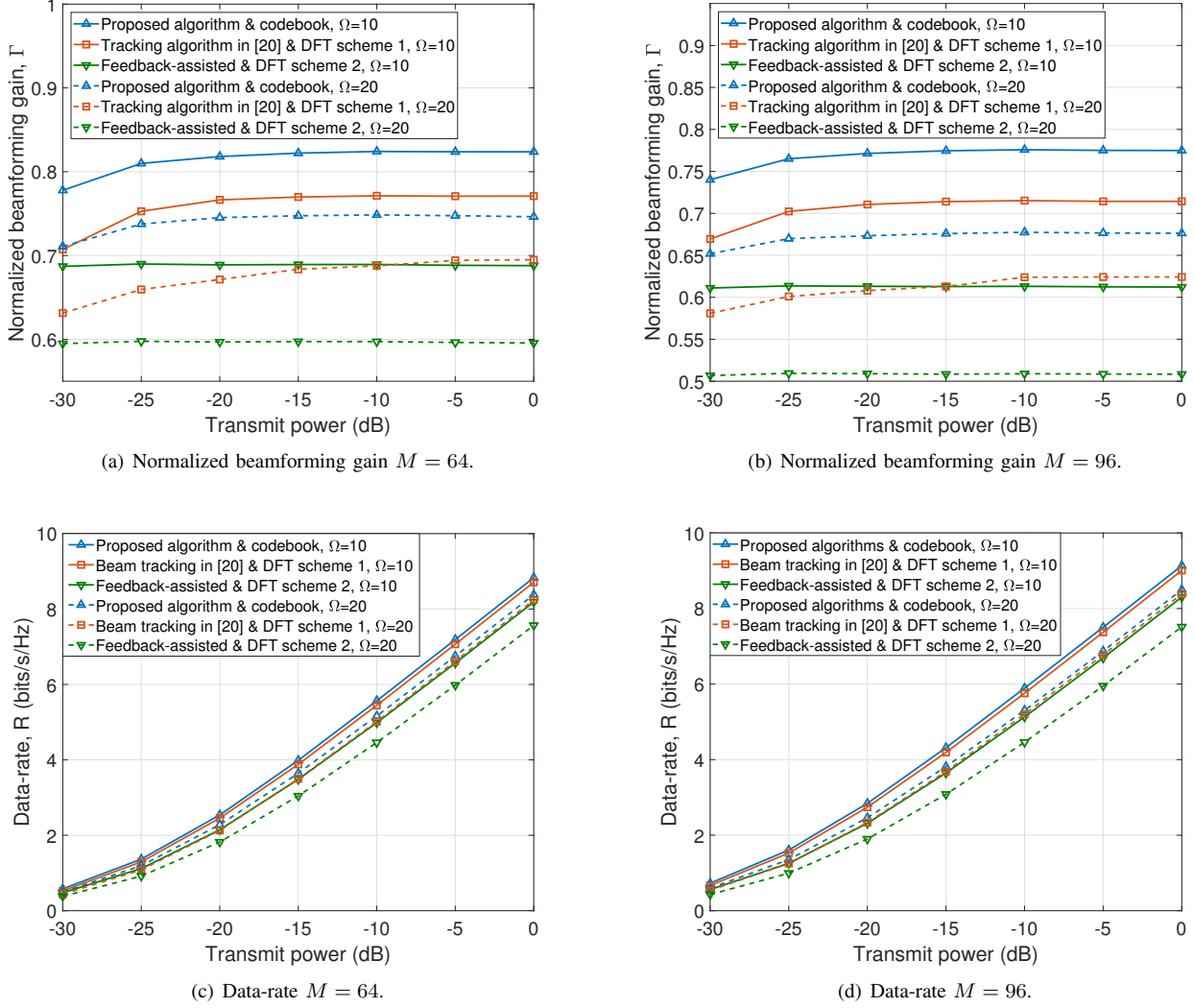


Fig. 11. Beamforming gain and data-rate of multi-resolution beamforming codebook ($\Omega = 10, 20$, $(Q_1, Q_2) = (\frac{M}{2}, M)$, $Q = \frac{3M}{2}$, $O = 2$, $\sigma_\epsilon = 0$).

In Figs. 9(a) and 9(b), the position and velocity tracking performances are evaluated using the normalized mean squared error (NMSE), $\Upsilon_x = E[|\frac{x_\ell - \hat{x}_\ell}{x_\ell}|^2]$ and $\Upsilon_v = E[|\frac{v_\ell - \hat{v}_\ell}{v_\ell}|^2]$, respectively. To check the effect of the initial feedback error, the standard deviation of the feedback error is set to $\sigma_\epsilon = [0, 10^{-1.5}, 10^{-1}]$. The simulation results show that a smaller NMSE can be achieved when the initial feedback error has less impact on the state vector. It is also shown that the NMSE decreases with increasing SNR, which implies that RSU can obtain measurement information with a high degree of reliability from the beginning of the vehicle tracking stage. Therefore, RSU puts more weight on the new measurement than the predicted state vector in order to obtain better estimates with less uncertainty. Moreover, Figs. 9 verify that the proposed algorithm outperforms the discrete Fourier transform (DFT) based beamforming solutions in [20] because it can adjust the beam-width of the beamformer according to the state estimation performance as well as to reduce the uncertainty in the state prediction process based on the acceleration estimation algorithm.

We evaluate the beamforming gain and system throughput of the proposed downlink beamforming algorithm based on the normalized beamforming gain, defined as $\Gamma \doteq E[|\mathbf{h}^H \mathbf{c}|^2 / \|\mathbf{h}\|_2^2]$ and the data-rate, defined as $R \doteq E[\log_2(1 + \rho_\ell |\mathbf{h}^H \mathbf{c}|^2)]$. The initial state vector is set to $\mathbf{t}_0 = [-50 \text{ m}, 8.5 \text{ m}, 60 \text{ km/h}]^T$. The normalized beamforming gain and the data-rate of the proposed vehicle tracking algorithm are compared with those of the vehicle tracking algorithm in [20] and those of the feedback-assisted state tracking approach. Communication systems relying on the DFT codebook are also considered in order to evaluate the beamforming performance of the proposed codebook. The transmit beamformer in DFT scheme 1 is chosen based on the estimated state vector $\tilde{\mathbf{t}}_{\tau + \frac{\Omega}{2}} = \mathbf{A}^{\frac{\Omega}{2}} \hat{\mathbf{t}}_\tau$ at time $\tau + \frac{\Omega}{2}$. Furthermore, the beamformer in DFT scheme 2 is chosen based on the state vector $\hat{\mathbf{t}}_\tau$, which is estimated at time τ .

We evaluate the beamforming gain and data-rate of the beamforming system with a single-resolution codebook including $Q = M$ codewords. Figs. 10 show that the proposed beamforming system provides higher performance than the

DFT-based beamforming systems because the codewords are designed by considering the road structure in which RSU is deployed. Further, we consider a beamforming system using a multi-resolution codebook consisting of a low-resolution codebook with $Q_1 = \frac{M}{2}$ codewords and a high-resolution codebook with $Q_2 = M$ codewords. As verified in Figs. 11, a beamformer with a narrow beam width is chosen to maximize the beamforming gain if the system determines that the state estimation performance is good. If the state estimation performance is poor, then a beamformer with a wide beam width is chosen to enhance the beam alignment performance. On the other hand, the DFT-based system cannot respond to change in the state estimation performance because it only exploits the beamformer with a single type of beam width. Also verified is that the performance gap between the proposed and DFT codebooks widens as the beamformer update period increases.

VI. CONCLUSION

In this paper, we developed a vehicle tracking algorithm that is suitable for seamless V2I communications in fast time-varying channels. Based on an EKF algorithm, we proposed a vehicle tracking algorithm to track the movement of vehicles using limited channel feedback resources. To realize reliable V2I communications with high beamforming gain, a beamforming codebook was designed by considering the road structure between the vehicle and RSU. Furthermore, we developed a beamformer selection algorithm to obtain a robust beamformer by predicting the future motion states of the vehicles. Simulation results demonstrated that the proposed vehicle tracking and downlink beamforming algorithms show improved beamforming gain and data-rate performance although they utilize fewer network resources than the feedback-assisted state tracking approach.

REFERENCES

- [1] N. Lu, N. Cheng, N. Zhang, S. X, and J. W. Mark, "Connected vehicles: Solutions and challenges," *IEEE internet of things journal*, vol. 1, no. 4, pp. 289–299, Mar. 2014.
- [2] Qualcomm, 5G NR based C-V2X, Std., 2018.
- [3] J. Zhang, F. Wang, K. Wang, W. Lin, X. Xu, and C. Chen, "Data-driven intelligent transportation systems: A survey," *IEEE Transactions on Intelligent Transportation Systems*, vol. 12, no. 4, pp. 1624–1639, Dec. 2011.
- [4] A. Rauch, F. Klanner, and K. Dietmayer, "Analysis of V2X communication parameters for the development of a fusion architecture for cooperative perception systems," in *Proceedings of IEEE Intelligent Vehicles Symposium*, Jun. 2011.
- [5] J. Choi, V. Va, N. Gonzalez-Prelcic, R. Daniels, C. R. Bhat, and R. W. Heath, "Millimeter-wave vehicular communication to support massive automotive sensing," *IEEE Communications Magazine*, vol. 54, no. 12, pp. 160–167, Mar. 2016.
- [6] TS-22.186, *Enhancement of 3GPP support for V2X scenarios*, 3GPP Std., 2019.
- [7] TS-22.185, *Service requirements for V2X services*, 3GPP Std.
- [8] TS-22.885, *Study on LTE support for vehicle to everything (V2X) services*, 3GPP Std.
- [9] P. Schulz, M. Matthé, H. Klessig, M. Simsek, G. Fettweis, J. Ansari, S. A. Ashraf, J. V. B. Almeroth, I. Riedel, A. Puschmann, A. Mitschele-Thiel, M. Müller, T. Elste, and M. Windisch, "Latency critical iot applications in 5G: Perspective on the design of radio interface and network architecture," *IEEE Communications Magazine*, vol. 55, no. 2, pp. 70–78, Feb. 2017.
- [10] G. Pocovi, H. Shariatmadari, G. Berardinelli, K. Pedersen, J. Steiner, and Z. Li, "Achieving ultra-reliable low-latency communications: Challenges and envisioned system enhancements," *IEEE Network*, vol. 32, no. 2, pp. 8–15, Apr. 2018.
- [11] J.-H. Lee and J. Song, "Full-duplex relay for millimeter wave vehicular platoon communications," *Sensors*, vol. 20, no. 21, pp. 1–15, Oct. 2020.
- [12] B. Antonescu, M. T. Moayyed, and S. Basagni, "Mmwave channel propagation modeling for V2X communication systems," in *Proc. IEEE PIMRC*, Oct. 2017.
- [13] Y.-P. Zhang, P. Wang, and A. Goldsmith, "Rainfall effect on the performance of millimeter-wave MIMO systems," *IEEE Transactions on Wireless Communications*, vol. 14, no. 9, pp. 4857–4866, Sep. 2015.
- [14] T. S. Rappaport, G. R. MacCartney, M. K. Samimi, and S. Sun, "Wideband millimeter-wave propagation measurements and channel models for future wireless communication system design," *IEEE Transactions on Communications*, vol. 63, no. 9, pp. 3029–3056, Sep. 2015.
- [15] J. Song, J. Choi, S. G. Larew, D. J. Love, T. A. Thomas, and A. Ghosh, "Adaptive millimeter wave beam alignment for dual-polarized MIMO systems," *IEEE Transactions on Wireless Communications*, vol. 14, no. 11, pp. 6283–6296, Nov. 2015.
- [16] V. Va, J. Choi, and R. W. Heath, "The impact of beamwidth on temporal channel variation in vehicular channels and its implications," *IEEE Transactions on Vehicular Technology*, vol. 66, no. 6, pp. 5014 – 5029, Jun. 2017.
- [17] S. Jayaprakasam, X. Ma, J. W. Choi, and S. Kim, "Robust beam-tracking for mmwave mobile communications," *IEEE Communications Letters*, vol. 21, no. 12, pp. 2654 – 2657, Dec. 2017.
- [18] V. Va, H. Vikalo, and R. W. Heath, "Beam tracking for mobile millimeter wave communication systems," in *IEEE Global Conference on Signal and Information Processing (GlobalSIP)*, Dec. 2016.
- [19] C. Zhang, D. Guo, and P. Fan, "Tracking angles of departure and arrival in a mobile millimeter wave channel," in *Proceedings of IEEE International Conference on Communications*, May 2016.
- [20] S. Shaham, M. Ding, M. Kokshoorn, Z. Lin, S. Dang, and R. Abbas, "Fast channel estimation and beam tracking for millimeter wave vehicular communications," *IEEE Access*, vol. 7, pp. 141 104–141 118, Sep 2019.
- [21] S. M. Kay, *Fundamentals of statistical signal processing: Estimation theory*. NJ: Prentice Hall, 1993.
- [22] G. A. Terejanu, "Extended Kalman filter tutorial," 2008.
- [23] J. Choi, D. J. Love, and P. Bidigare, "Downlink training techniques for fdd massive MIMO systems: Open-loop and closed-loop training with memory," *IEEE Journal of Selected Topics in Signal Processing*, vol. 8, no. 5, pp. 802–814, Dec. 2014.
- [24] S. G. Larew and D. J. Love, "Adaptive beam tracking with the unscented Kalman filter for millimeter wave communication," *IEEE Signal Processing Letters*, vol. 26, no. 11, pp. 1658–1662, Nov. 2019.
- [25] Z. Xiao, T. He, P. Xia, and X.-G. Xia, "Hierarchical codebook design for beamforming training in millimeter-wave communication," *IEEE Transactions on Wireless Communications*, vol. 15, no. 5, pp. 3380–3392, May 2016.
- [26] Z. Xiao, P. Xia, and X.-G. Xia, "Codebook design for millimeter-wave channel estimation with hybrid precoding structure," *IEEE Transactions on Wireless Communications*, vol. 16, no. 1, pp. 141–153, Jan. 2017.
- [27] S. Noh, M. D. Zoltowski, and D. J. Love, "Multi-resolution codebook and adaptive beamforming sequence design for millimeter wave beam alignment," *IEEE Transactions on Wireless Communications*, vol. 16, no. 9, 2017.
- [28] A. Alkhateeb, O. E. Ayach, and R. W. Heath, "Channel estimation and hybrid precoding for millimeter wave cellular systems," *IEEE Journal of Selected Topics in Signal Processing*, vol. 8, no. 5, pp. 831–846, Oct. 2014.
- [29] O. E. Ayach, S. Rajagopal, S. Abu-Surra, Z. Pi, and R. W. Heath, "Spatially sparse precoding in millimeter wave MIMO systems," *IEEE Transactions on Wireless Communications*, vol. 13, no. 3, pp. 1499–1513, Mar. 2014.
- [30] K. Saho, *Kalman filter for moving object tracking: Performance analysis and filter design*. InTech, 2018.
- [31] K. Petersen and M. Pedersen, "The matrix cookbook," Nov. 2012.
- [32] M. Borga, "Learning multidimensional signal processing," Ph.D. dissertation, Linköping University, Linköping, Sweden, 1998, SE-581 83.
- [33] L. Rebollo-Neira and D. Lowe, "Optimized orthogonal matching pursuit approach," *IEEE Signal Processing Letters*, vol. 9, no. 4, pp. 137–140, Dec. 2005.
- [34] J. Song, J. Choi, and D. J. Love, "Common codebook millimeter wave beam design: Designing beams for both sounding and communications with uniform planar arrays," *IEEE Transactions on Communications*, vol. 65, no. 4, pp. 745–754, Feb. 2017.

- [35] ——, “Codebook design for hybrid beamforming in millimeter wave systems,” in *Proceedings of IEEE International Conference on Communications*, Jun. 2015.
- [36] S. Kim, J. Choi, and J. Song, “Beam designs for millimeter-wave backhaul with dual-polarized uniform planar arrays,” *IEEE Transactions on Communications*, vol. 69, no. 7, pp. 4202–4217, Jul. 2020.
- [37] S. Hur, T. Kim, D. J. Love, J. V. Krogmeier, T. A. Thomas, and A. Ghosh, “Millimeter wave beamforming for wireless backhaul and access in small cell networks,” *IEEE Transactions on Communications*, vol. 61, no. 10, pp. 4391–4403, Oct. 2013.
- [38] J. Song, B. Lee, J. Park, M.-S. Lee, and J.-H. Lee, “Beamformer design for physical layer security in dual-polarized millimeter wave channels,” *IEEE Transactions on Vehicular Technology*, Nov. 2020.